# Improved nitrogen retrievals with airborne-derived fluorescence and plant traits quantified from VNIR-SWIR hyperspectral imagery in the context of precision agriculture

Carlos Camino[1], Victoria González-Dugo[1], Pilar Hernández[1], J.C. Sillero[2], Pablo J. Zarco-Tejada[1,*]

1. Instituto de Agricultura Sostenible (IAS), Consejo Superior de Investigaciones Científicas (CSIC), Alameda del Obispo s/n, 14004 Córdoba, Spain

2. Instituto Andaluz de Investigación y Formación Agraria, Pesquera, Alimentaria y de la Producción Ecológica (IFAPA), Centro Alameda del Obispo, s/n , 14004 Córdoba, Spain

***** Corresponding author

**Submitted to *International Journal of Applied Earth Observation and Geoinformation***
**February 2018**

**Abstract**

In semi-arid conditions, nitrogen (N) is the main limiting factor of crop yield after water, and its accurate quantification remains essential. Recent studies have demonstrated that solar-induced chlorophyll fluorescence (SIF) quantified from hyperspectral imagery is a reliable indicator of photosynthetic activity in the context of precision agriculture and for early stress detection purposes. The role of fluorescence might be critical to our understanding of N levels due to its link with photosynthesis and the maximum rate of carboxylation (Vcmax) under stress. The research presented here aimed to assess the contribution played by airborne-retrieved solar-induced chlorophyll fluorescence (SIF) to the retrieval of N under irrigated and rainfed Mediterranean conditions. The study was carried out at three field sites used for wheat phenotyping purposes in Southern Spain during the 2015 and 2016 growing seasons. Airborne campaigns acquired imagery with two hyperspectral cameras covering the 400–850 nm (20 cm resolution) and 950-1750 nm (50 cm resolution) spectral regions. The performance of multiple regression models built for N quantification with and without including the airborne-retrieved SIF was compared with the performance of models built with plant traits estimated by model inversion, and also with standard approaches based on single spectral indices. Results showed that the accuracy of the models for N retrieval increased when chlorophyll fluorescence was included ($r^2_{LOOCV} \geq 0.92$; $p<0.0005$) as compared to models only built with chlorophyll a+b ($C_{ab}$), dry matter ($C_m$) and equivalent water thickness ($C_w$) plant traits ($r^2_{LOOCV}$ ranged from 0.68 to 0.77; $p< 0.005$). Moreover, nitrogen indices (NIs) centered at 1510 nm yielded more reliable agreements with N concentration ($r^2=0.69$) than traditional chlorophyll indices (TCARI/OSAVI $r^2=0.45$) and structural indices (NDVI $r^2=0.57$) calculated in the VNIR region. This work demonstrates that under irrigated and non-irrigated conditions, indicators

directly linked with photosynthesis such as chlorophyll fluorescence improves predictions of N concentration.

**Keywords:** Nitrogen concentration, chlorophyll fluorescence, chlorophyll content, NIR indices, hyperspectral, airborne

## 1. Introduction

Nitrogen (N) content plays an important role in the plant life cycle. In most situations, N is the major limiting factor of crop yield after water deficiency, and it is an essential element in plant growth (Lemaire *et al*., 2008). It is well documented that an adequate N supply is crucial for the maintenance of plant biochemistry quality (Nobel, 2009), and that N deficiency greatly changes the photosynthetic capacity, leading to a decrease in photosynthetic quantum yield and light-saturated photosynthetic rate (Khamis *et al*., 1990). N management of crops has important economic impacts and environmental implications, although nitrogen overfertilization is widely used by farmers as a form of insurance against uncertain soil fertility (Tremblay *et al*., 2012). In particular, a higher N supply causes significant effects on the environment. Hence, an adequate N management strategy is needed to guide precision diagnosis of soil status and efficient crop management.

Traditionally, the N concentration is estimated using chemical analyses based on leaf tissue, such as Kjeldahl-digestion and Dumas-combustion, due to their reliability in organic N determination. However, these methods are destructive, time consuming, and need complex analysis. Moreover, traditional N estimates provide only limited information, as sampling is based on only a limited number of sites in a given field; they are therefore not suitable for the continuous monitoring of N content in the entire field. For these reasons, remote sensing and, in particular, hyperspectral imagery, can be useful for monitoring spatial and temporal variations in crop N content over large areas (Quemada *et al*., 2014).

The use of simple empirical models that incorporate hyperspectral reflectance indices is still the dominant method used to estimate N (Ferwerda *et al*., 2005; Stroppiana *et al*., 2009; Herrmann *et al*., 2010; Wang *et al*., 2012; Li *et al*., 2014; Mahajan *et al*., 2016).

Several studies have shown improvements in canopy N quantifications using reflectance bands in the near infrared (NIR) and in the short-wave infrared (SWIR) regions (Kokaly, 1999; Ferwerda *et al*., 2005; Herrmann *et al*., 2010; Pimstein *et al*., 2011; Gnyp *et al*., 2014; Mahajan *et al*., 2014), especially when indices calculated from wavelengths centered at 850 and 1510 nm are used, as described in detail by Herrmann *et al*. (2010). Serrano *et al*. (2002) also showed that the combination of the 1510 nm and 1680 nm spectral regions was sensitive to N concentration in green biomass. Nevertheless, and despite the successful empirical relationships, nitrogen estimation at the canopy level from remote sensing requires appropriate modeling strategies due to the large contribution of structural and shadow effects to canopy reflectance (Zarco-Tejada *et al*., 2005). On the other hand, radiative transfer models offer advantages compared to index-based empirical models regarding robustness and transferability (Jacquemoud and Baret, 1990; Zarco-Tejada *et al*., 2004; Schlerf and Atzberger, 2006; Wang *et al*., 2015), and these have been widely proposed as a method for retrieving chlorophyll content, dry matter, and water content from remote sensing data (Clevers and Kooistra, 2012; Jacquemoud and Baret, 1990; Zarco-Tejada *et al*., 2004). In this context, recent studies have evaluated the estimation of leaf N content using models built with leaf and canopy biophysical parameters retrieved by inversion (e.g. Wang *et al*., 2015), and these have yielded reasonable success ($r^2$= 0.58).

In recent years, the quantification of chlorophyll fluorescence has attracted increasing attention in the context of global monitoring of crop physiology and vegetation functioning, and this method can offer improvements on the estimation of N status (Tremblay *et al*., 2012). Chlorophyll fluorescence is generally considered as a direct proxy for electron transport rate and hence photosynthetic activity (Genty *et al.,* 1989; Weis and Berry, 1987).

78 The leaf-level maximum carboxylation rate (Vcmax; $\mu mol \cdot CO_2 \cdot m^{-2} \cdot s^{-1}$) is closely related to
79 the chlorophyll content at leaf scale (Croft *et al*., 2017; Houborg *et al*., 2013) and with
80 solar-induced chlorophyll fluorescence (SIF) (Rascher *et al.,* 2015; Yang *et al.,* 2015). In
81 this regard, SIF can be considered as a direct link with Vcmax through its strong connexion
82 to chlorophyll content and photosynthetic activity (Walker *et al.,* 2014). In fact, recent
83 studies have demonstrated the link between chlorophyll fluorescence and photosynthetic
84 activity at leaf and canopy levels (see e.g. Zarco-Tejada *et al*., 2013, 2016; Cendrero-Mateo
85 *et al*., 2016). The rationale is based on the dependence of chlorophyll fluorescence
86 emissions on chlorophyll concentration and photosystem I (PSI) and II (PSII) efficiency
87 (Lichtenthaler *et al*., 1996). It is well documented that N deficiency affects PSII
88 photochemistry, lowering the quantum yield electron transport, the photochemical
89 efficiency, and therefore the assimilation rate (Lu and Zhang, 2000; Jin *et al*., 2015).
90
91 Crop water status may alter N balance: crop N demand is reduced under drought
92 conditions, as growth rate diminishes (Gonzalez-Dugo *et al.* 2010). In arid and semi-arid
93 environments, the co-limitation between nitrogen and water often reduces crop production
94 which therefore must be considered together (Sadras, 2004). For these reasons, spectral
95 indicators related to the leaf functioning, as chlorophyll fluorescence, is a potentially
96 important candidate for improving the quantification of N concentration using passive
97 remote sensing techniques. The present study aimed to explore the contribution of airborne-
98 retrieved chlorophyll fluorescence to the quantification of N concentration using
99 hyperspectral imagery. Specifically, we evaluated the fluorescence quantification in spring
100 wheat (early sawing) grown under rainfed and irrigated conditions to assess whether they

101 contributed significantly to the retrieval of N concentration in the context of precision
102 agriculture and plant phenotyping experiments.
103
104 **2. Material and Methods**
105 ***2.1. Study area***
106 The study was carried out in 2015 and 2016 at three field trial sites for durum wheat
107 (*Triticum turgidum L. var. durum)* and bread wheat (*Triticum aestivum L.)* selection in
108 Southern Spain. The sowing date for all sites was mid-November in the previous year.
109 Regarding fertilization, pest and disease management, all the plots received the same
110 treatment at all trial sites. Fertilization with diammonium phosphate and urea was carried
111 out in early November, while similar amounts of fungicides and pesticides were applied at
112 the early and middle growth stages at all trial sites.
113
114 The first trial site was located in Ecija (EC), near Seville, Southern Spain (*37°32'17"N,*
115 *5°06'57"W*), which was managed under rainfed conditions in 2015. The experiment was
116 designed with a balanced square lattice design using 300 individual plots (6 x 1.25 meters)
117 separated in four blocks, with 150 varieties of durum wheat and 150 of bread wheat. Each
118 cultivar was replicated three times per block (Fig. 1a).
119
120 The second site trial was in Carmona (CA), also close to Seville, Southern Spain
121 (*37°30'29"N, 5°34'42"W*) in 2015. The experiment comprised 882 individual plots
122 (7.5x1.25 meters) divided into two blocks managed under rainfed conditions and one block
123 under irrigated conditions. Each block contained a mixture of varieties of durum and bread
124 wheat, each cultivar replicated three times per block (Fig. 1b).

125

126 The third trial site was managed by IFAPA in Santaella (SA), near Cordoba, Southern
127 Spain (*37°31'34"N, 4°50'40"W*) in 2016, where 20 varieties of durum wheat and 20
128 varieties of bread wheat were replicated three times under irrigated and rainfed conditions
129 (Fig. 1c). The plot size was 15 $m^2$ (10 x 1.5 meters).

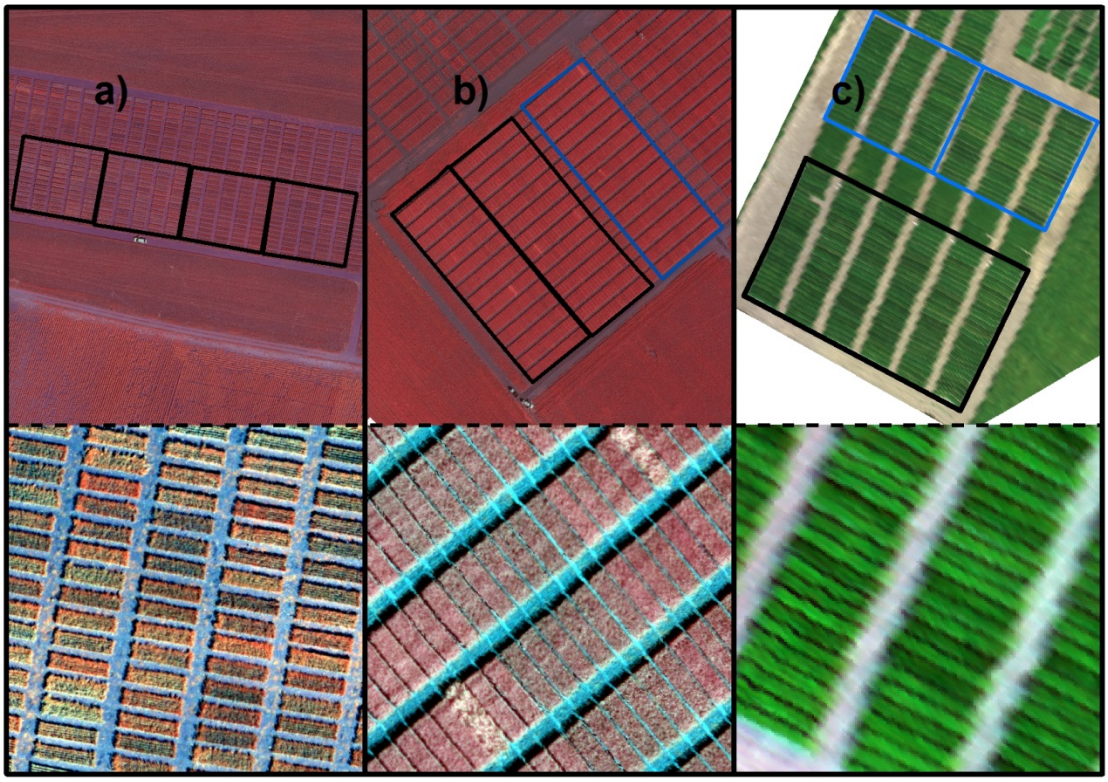


**Fig. 1**. Scene of the field trial sites at EC (a), CA (b) and Santaella (c) obtained with a color infrared camera (CIR; a and b, not used for analysis in this study) and the hyperspectral imagery (c) on board the aircraft. Black rectangles indicate plots under rainfed conditions and blue rectangles indicate plot under irrigated conditions.

130 ***2.2. Field data***

131 In order to assess the physiology and the leaf optical properties of the wheat, a series of
132 leaf-level measurements were made concurrently with the airborne flights at midday (12:00
133 to 13:00 h local time) at all the trial sites. A summary of field measurements and airborne

campaigns at each trial site is shown in Table 1. The wheat growth stage during the flight campaigns refers to the stem length at the time of the first flight in Santaella (SA-1) and grain filling (milking stage) at the time of the flights in EC, CA and the second flight in Santaella (SA-2).

Leaf water potential ($\psi_L$; MPa) was measured using a pressure chamber (Model 600 Pressure Chamber Instrument, PMI Instrument Company, Albany, NY, USA) on two sunlit leaves per plot. Assimilation rate (A; $\mu mol \cdot m^{-2} \cdot s^{-1}$) and stomatal conductance (Gs; $mmol \cdot m^{-2} \cdot s^{-1}$) were measured using a photosynthesis measurement system (LCDpro-SD, ADC Bioscientific Ltd., Herts, UK) on two sunlit leaves per plot. Steady-state leaf fluorescence yield (Ft) and a SPAD chlorophyll content indicator were measured on 10 to 15 leaves per plot using a FluorPen FP100 (Photon Systems Instruments, Brno, Czech Republic) and a chlorophyll meter (SPAD-502, Minolta Corp., Ramsey, NJ, USA), respectively. The relationship between chlorophyll concentration and SPAD readings for wheat found by Uddling *et al*. (2007) was applied to convert SPAD data into chlorophyll content ($\mu g \cdot cm^{-2}$). Total N concentration was determined by the Kjeldhal method (Kjeldahl, 1883) on 20-25 sunlit leaves sampled per plot. As in the rest of the physiological measurements, a random selection of the sunlit leaves was carried out from the central area of each plot.

**Table 1**. Field measurements and flight dates during the 2015 and 2016 campaigns.

| Year | Site | Flight dates | Type of flight (a) | Field measurements | Plots with field data |
|---|---|---|---|---|---|
| **2015** | EC | 28/05 | Noon (T + VNIR +SWIR) | $\psi_L$, A, Gs, Ft, SPAD, N | 12 (b) |
| | CA | 30/05 | Noon (T + VNIR +SWIR) | $\psi_L$, A, Gs, Ft, SPAD, N | 18 (b) |
| **2016** | SA-1 | 17/03 | Noon (T + VNIR +SWIR) | $\psi_L$, A, Gs, Ft, SPAD, N | 24 (b) and 45(c) |
| | SA-2 | 26/04 | Noon (T + VNIR +SWIR) | $\psi_L$, A, Gs, Ft, SPAD, N | 24 (b) and 50(c) |

**a** T= thermal camera, VNIR = hyperspectral visible and infrared camera (400-885 nm), SWIR = hyperspectral near-infrared and short-wave infrared camera (950-1750 nm).
**b** number of plots with all leaf measurements
**c** number of plots with only measurements of SPAD and total leaf nitrogen.

### *2.3. Airborne hyperspectral imagery*

A hyperspectral imager covering the visible and near-infrared region (Micro-Hyperspec VNIR, Headwall Photonics, Fitchburg, MA, USA) and a second hyperspectral imager covering the NIR and the SWIR regions (Micro-Hyperspec NIR-100, Headwall Photonics) were installed in tandem on a Cessna aircraft operated by the Laboratory for Research Methods in Quantitative Remote Sensing (QuantaLab), Consejo Superior de Investigaciones Científicas (IAS-CSIC, Spain). Imagery was acquired at 250 m above ground level with the aircraft flying on the solar plane during the flight campaigns of 2015 and 2016. The campaigns were flown at midday (local time) to minimize differences due to sun angle effects between flights.

The micro-hyperspec VNIR was set up with a configuration of 260 spectral bands acquired at 8 nm/pixel and 12-bit radiometric resolution in the 400–885 nm spectral region, thus

yielding a 6.4 nm Full Width at Half Maximum (FWHM) with a 25-μm slit. The acquisition and storage module had a 50 fps frame rate with an integration time of 25 ms. The 8-mm focal length lens yielded an IFOV of 0.93 mrad and an angular FOV of 50° with a spatial resolution of 20 cm (Fig. 2a) (further information regarding the setup of micro-hyperspec VNIR can be obtained from Zarco-Tejada *et al*., 2016).

The micro-hyperspec NIR-100 camera was flown with a configuration of 165 spectral bands and 16-bit radiometric resolution in the spectral region of 950 to 1750 nm, yielding 6.05 nm FWHM with a 25-μm slit and an optical aperture of f/1.4. The FWHM and the center wavelength for each spectral band were derived after spectral calibration using a Cornerstone 260 1/4m Monochromator (model 74100; Oriel Instruments, USA) and the XE-1 Xenon Calibration Light Source (Oceanic Optics, USA). The frame rate on board the aircraft was set to 50 fps with an integration time of 40 ms. The 12.5-mm focal length lens yielded an angular FOV of 38.6º with a spatial resolution of 60 cm (Fig. 2b).

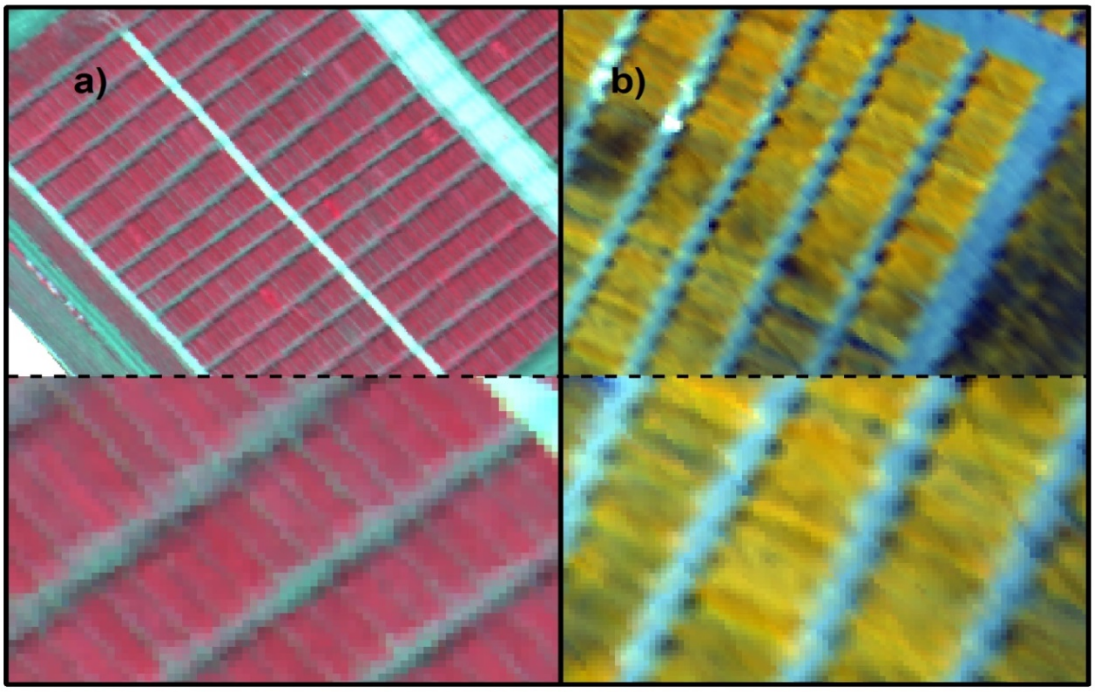


**Fig. 2**. Sample hyperspectral VNIR (400-800 nm region) (a) and hyperspectral NIR (900-1700 nm region) (b) imagery acquired during the 2015 and 2016 airborne campaigns performed at the trial sites at CA and SA-1, respectively. The central region of the plot was used to calculate hyperspectral indices and to quantify chlorophyll fluorescence.

185 Radiometric calibration of the hyperspectral cameras and ortho-rectification of the imagery
186 were carried out as described by Zarco-Tejada *et al*. (2016). Atmospheric correction of the
187 imagery was performed using aerosol optical depth (AOD) and weather data to simulate the
188 incoming irradiance using the SMARTS model (Gueymard, 1995; Gueymard *et al*., 2002),
189 measured in the field concurrently with the airborne flights. The SMARTS model has been
190 used in previous studies to calculate reflectance from both multispectral and hyperspectral
191 imagery (Berni *et al*., 2009; Zarco-Tejada *et al*., 2012, 2016; Calderón *et al*., 2013, 2015).
192 A further step was carried out to apply an empirical line calibration (Smith and Milton,
193 1999) using field-measured spectra to remove noise. The average radiance and reflectance
194 values of selected wheat plots from each trial site are shown in Fig. 3.

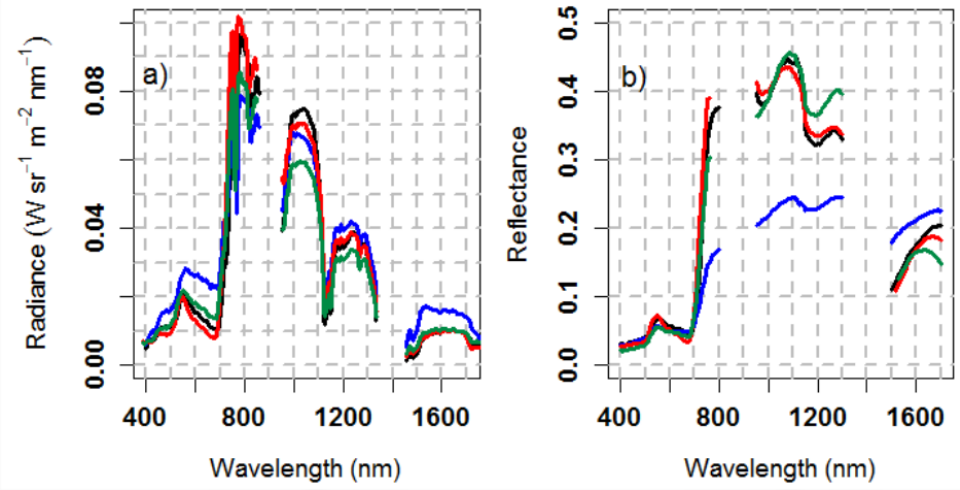


**Fig. 3**. Mean radiance in $W \cdot sr^{-1} \cdot m^{-2} \cdot nm^{-1}$ (a) and reflectance spectra (b) retrieved from hyperspectral cameras at EC (in blue), CA (in black), SA-1(in red) and SA-2 (in Green).

### *2.4. Fluorescence retrieval and calculation of narrow-band indices from the airborne hyperspectral imagery*

The atmospheric $O_2$-A oxygen absorption band at 760.5 nm was used for the fluorescence retrieval via the *in-filling* method. In particular, the Solar Induced Fluorescence (SIF) was quantified from the radiance spectra (Fig. 3a) using the Fraunhofer Line Depth (FLD) principle (Plascyk, 1975) as described in Zarco-Tejada *et al*. (2013; 2016). The SIF signal calculated using the *in-filling* method was based on two spectral bands *in* and *out* the $O_2$-A feature, as described in Meroni *et al*. (2010). The FLD2 method used in this study extracted the radiance $L_{in}$ (L762 nm) and $L_{out}$ (L750 nm) from the airborne imagery, and the irradiance $E_{in}$ (E762 nm) and $E_{out}$ (E750 nm) from irradiance spectra concurrently measured at the time of the flights. Measurements were made using an ASD Field Spectrometer (FieldSpec Handheld Pro, ASD Inc., CO, USA) with a cosine corrector-diffuser probe for

207 the entire 400-1000 nm spectral region. A modelling study by Damm et al. (2011)
208 quantified the effects of the spectral sampling interval, spectral resolution, signal to noise
209 ratio (SNR) and the spectral shift on the accuracy of the fluorescence retrieval using the $O_2$-
210 A feature. They demonstrated the feasibility of the SIF retrieval via the FLD methods with
211 broader spectral bandwidths (i.e., 5-7 nm FWHM) when high spectral sampling (below 2.5
212 nm) and SNR higher than 300:1 were available. These results agree with the fluorescence
213 retrievals shown in Zarco-Tejada et al. (2012) and later in Damm *et al.* (2015) with APEX.
214 According to these works, the hyperspectral configuration used in this study is suitable for
215 the SIF retrievals (1.85 nm sampling interval, 6.4 nm bandwidths and SNR of 300:1 with
216 spatial binning).
217
218 Narrow-band indices were calculated from the average reflectance per plot using the 260
219 spectral bands acquired by the micro-hyperspec VNIR, and from the 164 spectral bands
220 acquired by the micro-hyperspec NIR cameras (Fig. 3b). In the SWIR region, the
221 atmospheric water absorption spectral region (1330–1490 nm) was masked before analysis.
222 Table 2 groups the vegetation indices (VIs) calculated from the micro-hyperspec VNIR into
223 four categories related to: 1) structure, 2) chlorophyll concentration, 3) chlorophyll
224 fluorescence, and 4) nitrogen indices (NIs) using NIR and SWIR spectral domains.

**Table 2**. Summary of the vegetation indices using the VNIR (400-800 nm region) and NIR (900-1700 nm region) hyperspectral airborne imagery.

| Indices | Equation | Reference |
|---|---|---|
| **Structural indices** | | |
| Normalized Diff. Veg. Index | $NDVI=(R_{800}-R_{670})/(R_{800}+R_{670})$ | Rouse *et al*. (1973) |
| Opt. Soil-Adjusted Veg. Index | $OSAVI=(1+0.16)(R_{800}-R_{670})/(R_{800}+R_{670}+0.16)$ | Rondeaux *et al*. (1996) |
| Renormalized Diff. Veg. Index | $RDVI=(R_{800}-R_{670})/(R_{800}+R_{670})^{0.5}$ | Roujean and Breon (1995) |
| MCARI/MTVI2 | MCARI/MTVI2 | Eitel *et al*. (2007) |
| **Chorophyll *a+b* indices** | | |
| Transf. Chl. Absorp. Rfl. Index | $TCARI = 3[(R_{700}-R_{670})-0.2(R_{700}-R_{550})(R_{700}/R_{670})]$ | Haboudane *et al*. (2002) |
| TCARI/OSAVI | TCARI/OSAVI | Haboudane *et al*. (2002) |
| Mod. Chl. Absorp. Rfl. Index | $MCARI = [(R_{700}-R_{670})-0.2(R_{700}-R_{550})](R_{700}/R_{670})$ | Daughtry *et al*. (2000) |
| Pig. Spec. Simpl. Ratio Chl. b | $PSSRb = R_{800}/R_{635}$ | Blackburn (1998) |
| Gitelson and Merzlyak Indices | $GM1=R_{750}/R_{550}$; $GM2=R_{750}/R_{700}$ | Gitelson and Merzlyak (1997) |
| Vogelmann Index | $VOG=R_{740}/R_{720}$ | Vogelmann *et al*. (1993) |
| Red-edge CI | $CI=R_{750}/R_{710}$ | Zarco-Tejada *et al*. (2001) |
| **Chlorophyll fluorescence (SIF)** | | |
| SIF | FLD2=d-Rb; where $d=L_{762}$; $R=(L_{762}-L_{750})/(E_{762}-E_{750})$ and $b=E_{762}$ | Moya *et al*. (2004); Plascyk and Gabriel (1975) |
| **Nitrogen indices (NIs)** | | |
| Double-peak C. N | $DCNI=(R_{720}-R_{700})(R_{700}-R_{670})/(R_{720}-R_{670})+0.3)$ | Chen *et al*. 2010 |
| $TCARI_{1510\ nm}$ | $TCARI_{1510}=3[(R_{700}-R_{1510})-0.2(R_{700}-R_{550})](R_{700}/R_{1510})$ | Herrmann *et al*. 2010 |
| $TCARI/OSAVI_{1510\ nm}$ | $TCARI_{1510}/OSAVI_{1510}= TCARI_{1510}/[(1+L)(R_{800}-R_{1510})/(R_{800}+R_{1510}+L)]$ | Herrmann *et al*. 2010 |
| $MCARI_{1510\ nm}$ | $MCARI_{1510}= [(R_{700}-R_{1510})-0.2(R_{700}-R_{550})](R_{700}/R_{1510})$ | Herrmann *et al*. 2010 |
| GnyLi | $GnyLi=(R_{900}*R_{1050})(R_{955}*R_{1220})/(R_{900}*R_{1050})+(R_{955}*R_{1220})$ | Gnyp *et al*. 2014 |
| Norm. Diff. N. Index | $NDNI=\log(1/R_{1510})-\log(1/R_{1680})/(\log(1/R_{1510})+\log(1/R_{1680})$ | Serrano *et al*. 2002 |
| $N_{1645,1715}$ | $N_{1645,1715}=(R_{1645}-R_{1715})/(R_{1645}+R_{1715})$ | Pimstein *et al*. 2011 |
| $N_{870,1450}$ | $N_{870,1450}=(R_{870}-R_{1450})/(R_{870}+R_{1450})$ | Pimstein *et al*. 2011 |
| $N_{850,1510}$ | $N_{850,1510}=(R_{850}-R_{1510})/(R_{850}+R_{1510})$ | This study |

### *2.5. Modelling methods*

Radiative transfer simulations were carried out with PROSPECT (Jacquemoud and Baret, 1990) linked to the SAILH model (Baret *et al*., 1992). Biophysical canopy parameters by means of numerical model inversion were estimated using look-up tables (LUT). The input

229 variables and their ranges in PROSPECT and SAILH models are shown in Table 3. The
230 viewing geometry, defined by the solar zenith and azimuth, and the viewing angles needed
231 to simulate canopy reflectance were extracted for each flight date. In order to minimize the
232 impact of the viewing geometry at each flight date and time, a step of five degrees around
233 the solar zenith angle during the flights was applied to the PROSPECT-SAILH radiative
234 transfer model inversions.

**Table 3**. Ranges of the main variables used in the PROSPECT-SAILH radiative transfer model inversions.

| Model | Symbol | Quantity | Ranges | Step | Unit |
|---|---|---|---|---|---|
| **PROSPECT** | N-struct | Leaf structure parameter | 1.25-1.85 | 0.1 | … |
| | $C_{ab}$ | Chlorophyll a +b content | 10-70 | 0.5 | µg $cm^{-2}$ |
| | $C_w$ | Equivalent water thickness | 0.001-0.05 | 0. 0005 | g $cm^{-2}$ |
| | $C_m$ | Dry matter content | 0.001-0.05 | 0. 0005 | g $cm^{-2}$ |
| | $C_s$ | Brown pigment content | 0 | … | … |
| | Sl | Hot-spot parameter | 0.001 | … | … |
| **SAILH** | LAI | Leaf area index | 2-5 | 0.1 | … |
| | LADF | Leaf inclination distribution function | 1,2,3 and 4* | … | … |
| | TV | Solar zenith angle | 45º,60º,85º | 5 | deg |
| | Phi | Viewing zenith angle | 0º | … | deg |
| | PSR | Relative azimuth angle | 0º | … | deg |

* Canopy types proposed to define LADF: planophile (1), erectophile (2), plagiophile (3) and spherical (4).

235 In this study two standard model inversions and one inversion method by steps were
236 performed. The range of variation for $C_{ab}$ was determined on the basis of prior field
237 information. In the standard model inversion method, the chlorophyll a+b, water and dry
238 matter content were estimated at the same time, while in the inversion method by steps, the
239 estimation of biophysical canopy parameters required consecutive steps (e.g.; as in Wang *et*
240 *al*., 2015). The spectral range between 400 and 800 nm measured with the micro-hyperspec
241 VNIR camera was used in the standard model inversion method (named here as INV-1),

242 while the entire spectral region (400 to 1700 nm) from both hyperspectral VNIR and NIR-
243 100 cameras was used in the full-range inversion (here called INV-2) and in the inversion
244 model by steps. In the inversion by steps, the main input parameters were calculated using
245 specific spectral ranges where the biophysical parameters have the greatest influence on the
246 reflectance and transmittance. The procedure was conducted as follows: 1) leaf angle
247 distribution function (LADF) was estimated over the entire spectral domain (400-1750 nm)
248 with variables $C_{ab}$, $C_w$ and $C_m$ according to Table 3. LADF was firstly retrieved by model
249 inversion, given its key role on canopy structure; 2) the mesophyll structure parameter (N-
250 struct) and leaf area index (LAI) were simultaneously determined over the range 960–1300
251 nm once the LADF had been fixed to the value retrieved in the first step, and with variable
252 $C_{ab}$, $C_w$ and $C_m$ according to Table 3; 3) $C_{ab}$ was determined over the range 455–690 nm,
253 with $C_w$ and $C_m$ according to Table 3, fixing LADF, LAI and N determined in previous
254 steps; 4) $C_w$ and $C_m$ were concurrently retrieved over 900–1700 nm, where water and dry
255 matter have the largest absorption effects (Baret and Fourty, 1997; Feret *et al*., 2008;
256 Fourty *et al*., 1996; Jacquemoud *et al*., 2009, 1996).
257
258 The accuracy of the estimated parameters (LADF, N-struct, LAI, $C_{ab}$, $C_w$ and $C_m$) via
259 model inversion was evaluated by the RMSE calculated between the simulated and
260 measured canopy spectral reflectance. For each standard model inversion, a total of 500000
261 inversions were carried in forward mode, whereas a total of 200000 inversions were used
262 for the inversion method by steps. Finally, the coefficient of determination ($r^2$) was
263 calculated to investigate the relationship between the retrieved biophysical parameters ($C_{ab}$,
264 $C_w$ and $C_m$) obtained by PROSPECT-SAILH model inversion and the ground-truth
265 physiological measurements.

### *2.6. Statistical analysis*

Stepwise multiple regression analysis using forward mode and leave-one-out-cross-validation (LOOCV) techniques were employed to select the best model to quantify N concentration using i) biophysical parameters derived from the different model inversion methods described above, ii) using narrow-band spectral indices calculated from the VNIR and NIR-100 hyperspectral imagery; and iii) evaluating the performance of the models with the addition of chlorophyll fluorescence quantified from the hyperspectral imagery. Therefore, statistical tests were employed to assess the robustness of each regression model built for nitrogen quantification with and without including solar-induced fluorescence emission retrieved from hyperspectral imagery. A residual analysis model was used to assess the independence of the residual, and the Shapiro-Wilk test for homoscedasticity to verify the normal distribution. The F-test was used to test the significance of the linear regression model, and Student's t-test for the significance of individual regression coefficients. Independent data sets were used for the statistical analysis, using a training data set to build a multiple regression, and an independent second data set to assess the performance of each model under rainfed and irrigated conditions. The training data set comprised the plots located in EC, CA and SA-1, in which the main physiological measurements were made. The test data set was built by SA-1 and SA-2 plots and separated under rainfed and irrigated conditions.

The mean absolute error (MAE), root mean square error (RMSE), mean percentage error (MPE), mean absolute percentage error (MAPE) and coefficient of determination ($r^2$) between the measured leaf nitrogen content and predicted values were used as skill scores

to validate the performance of each model. The statistical analysis was conducted in R software (R Core Team, 2015).

## 3. Results

### *3.1. Field measurements*

Mean values of the field physiological measurements and chlorophyll fluorescence retrieved from the airborne imagery for each field site under rainfed and irrigated conditions are shown in Table 4. The results revealed wide variations in the crop physiological status on all sites. As expected, the irrigated plots displayed overall better water and nutritional status than the rainfed plots. There were differences among the rainfed plots; average values of mean N concentration, assimilation rate (A), $G_s$, and SIF were lower in EC and SA-2 compared to CA and SA-1 (Table 4). The irrigated plots at SA-1, which were at an earlier stage of growth, and at SA-2, displayed an overall better water and nutritional status. These data confirmed the water and nutrient stress conditions in rainfed plots and a large variability among plots.

**Table 4**. Average N concentration (%), chlorophyll content derived from SPAD ($C_{ab}$; $\mu g \cdot cm^{-2}$), net assimilation (A; $\mu mol \cdot m^{-2} \cdot s^{-1}$), stomatal conductance (Gs; $mmol \cdot m^{-2} \cdot s^{-1}$), leaf-water potential ($\psi L$; MPa) and chlorophyll fluorescence (SIF in in $Watt \cdot sr^{-1} \cdot m^{-2} \cdot nm^{-2}$), under rainfed and irrigated conditions at EC, CA, SA-1 and SA-2. The standard deviation is also shown.

| | N concentration | $C_{ab}$ (SPAD) | A | $G_s$ | $\psi_L$ | SIF |
|---|---|---|---|---|---|---|
| **Rainfed** | | | | | | |
| **EC** | 2.50±0.46 | 23.4±3.7 | 7.7± 2.1 | 61.27±2 | -2.3±0.2 | 3.74±0.62 |
| **CA** | 3.28±0.34 | 28.0±3.6 | 11.3±2.1 | 71±24.8 | -2.5±0.4 | 4.22±0.25 |
| **SA-1** | 4.17±0.19 | 35.0±3.2 | 17.0±3.3 | 185.8±56.1 | -2.4±0.2 | 4.88±0.57 |
| **SA-2** | 2.63±0.32 | 26.0±2.4 | 10.0±2.5 | 121.8±40.5 | -2.7±0.2 | 4.01±0.40 |
| **Irrigated** | | | | | | |
| **CA** | 3.37±0.04 | 28.5±2.3 | 14.7±4.1 | 270.6±65.4 | -2.1±0.1 | 4.38±0.17 |
| **SA-1** | 4.29±0.28 | 35.8±4.1 | 24.4±2.4 | 354.6±109.4 | -1.7±0.2 | 5.71±0.29 |
| **SA-2** | 2.95±0.31 | 29.3±3.9 | 18.3±2.4 | 283.2±65.2 | -2.2±0.1 | 5.14±0.28 |

### *3.2. Nitrogen concentration and narrow-band hyperspectral indices*

The solar induced fluorescence emission and narrow-band reflectance indices calculated from hyperspectral imagery were assessed against field measurements of nitrogen content, chlorophyll content measured with SPAD, and net assimilation (Table 5). The results showed that the NIR/SWIR-based NIs were marginally better predictors of nitrogen content than the VNIR indices, with the $MCARI_{1510}$ and the NDNI (Fig. 4a) indices yielding the best correlation with nitrogen content ($r^2$=0.69; p-value ≤ 0.005) as compared to MCARI ($r^2$=0.63) and PSSRb ($r^2$=0.63). The NIs that were modified to replace the 670nm band by the 1510 nm band due to its relationship with nitrogen absorption ($TCARI_{1510}$, $MCARI_{1510}$, $TCARI/OSAVI_{1510}$) performed higher at quantifying canopy nitrogen content than their

corresponding VNIR-based indices. The $N_{1645/1715}$ using exclusively reflectance in the SWIR domain showed significant relationship with N content ($r^2$=0.64, p-value<0.005) but still marginally inferior to $MCARI_{1510}$ and NDNI. Table 5 also shows that the indices most sensitive to canopy structure yielded significant relationships with nitrogen content ($r^2$=0.57; p-value <0.005; NDVI). However, the structural indices exhibited saturation over dense canopy, as shown in Fig. 4b for NDVI which tends to saturate due to the higher canopy density at high nitrogen levels. Among the chlorophyll indices used in this study, PSSRb (Fig. 4c) obtained the best results for chlorophyll content estimation ($r^2$=0.57, p-value $\leq$ 0.0005), yielding better results than NIs. The airborne-quantified chlorophyll fluorescence was also sensitive to nitrogen content ($r^2$=0.51; p-value $\leq$ 0.005) and to the assimilation rate ($r^2$=0.74; p-value $\leq$ 0.005; Fig. 4d), confirming other studies that demonstrated the link between airborne-retrieved chlorophyll fluorescence and the photosynthetic activity.

**Table 5**. Coefficient of determination ($r^2$) and level of significance for the narrow-band hyperspectral indices and the solar induced chlorophyll fluorescence (SIF; $Watt \cdot m^{-2} \cdot sr^{-1} \cdot nm^{-1}$) quantified from hyperspectral imagery against N concentration, chlorophyll content derived from SPAD values ($C_{ab}$-SPAD; $\mu g \cdot cm^{-2}$) and net assimilation (A; micromol/$m^2$/s).

| | N concentration | | $C_{ab}$-SPAD | | Net assimilation (A) | |
|---|---|---|---|---|---|---|
| **Indices** | **$r^2$** | **p-value** | **$r^2$** | **p-value** | **$r^2$** | **p-value** |
| **Structural Indices** | | | | | | |
| **NDVI** | 0.57 | < 2.2e-16 | 0.53 | < 2.2e-16 | 0.55 | 1.61E-08 |
| **OSAVI** | 0.56 | < 2.2e-16 | 0.49 | < 2.2e-16 | 0.53 | 3.23E-08 |
| **RDVI** | 0.56 | < 2.2e-16 | 0.48 | < 2.2e-16 | 0.53 | 3.92E-08 |
| **MCARI/MTVI2** | 0.40 | 2.14E-13 | 0.25 | 2.14E-13 | 0.46 | 5.61E-07 |
| **Chlorophyll a+b indices** | | | | | | |
| **TCARI** | 0.54 | < 2.2e-16 | 0.51 | < 2.2e-16 | 0.60 | 1.02E-09 |
| **TCARI/OSAVI** | 0.45 | 1.78E-15 | 0.30 | 8.64E-10 | 0.51 | 8.59E-08 |
| **MCARI** | 0.63 | < 2.2e-16 | 0.55 | < 2.2e-16 | 0.57 | 4.78E-09 |
| **PSSRb** | 0.63 | < 2.2e-16 | 0.57 | < 2.2e-16 | 0.66 | 3.72E-11 |
| **GM1** | 0.36 | 8.32E-12 | 0.39 | 2.90E-13 | 0.47 | 3.62E-07 |
| **GM2** | 0.52 | < 2.2e-16 | 0.47 | 2.22E-16 | 0.26 | 4.79E-04 |
| **VOG1** | 0.35 | 4.65E-10 | 0.32 | 1.75E-10 | 0.66 | 3.72E-11 |
| **CI** | 0.31 | 1.31E-11 | 0.35 | 1.48E-11 | 0.47 | 3.62E-07 |
| **Nitrogen Indices** | | | | | | |
| **DCNI** | 0.56 | < 2.2e-16 | 0.50 | < 2.2e-16 | 0.59 | 1.77E-09 |
| **$TCARI_{1510}$** | 0.56 | < 2.2e-16 | 0.44 | 1.78E-15 | 0.59 | 1.57E-09 |
| **$TCARI/OSAVI_{1510}$** | 0.52 | 2.35E-18 | 0.41 | 7.47E-14 | 0.63 | 2.26E-10 |
| **$MCARI_{1510}$** | 0.69 | < 2.2e-16 | 0.56 | < 2.2e-16 | 0.43 | 1.86E-06 |
| **GnyLi** | 0.31 | 3.41E-10 | 0.31 | 2.36E-10 | 0.51 | 7.98E-08 |
| **NDNI** | 0.69 | < 2.2e-16 | 0.49 | < 2.2e-16 | 0.61 | 5.75E-10 |
| **$N_{1645}$** | 0.64 | < 2.2e-16 | 0.52 | < 2.2e-16 | 0.59 | 1.57E-09 |
| **$N_{850-1450}$** | 0.64 | < 2.2e-16 | 0.55 | < 2.2e-16 | 0.63 | 2.26E-10 |
| **$NI_{850/1510}$** | 0.65 | < 2.2e-16 | 0.53 | < 2.2e-16 | 0.61 | 5.75E-10 |
| **Fluorescence** | | | | | | |
| **SIF** | 0.51 | < 2.2e-16 | 0.35 | 1.37E-11 | 0.74 | 1.19E-11 |

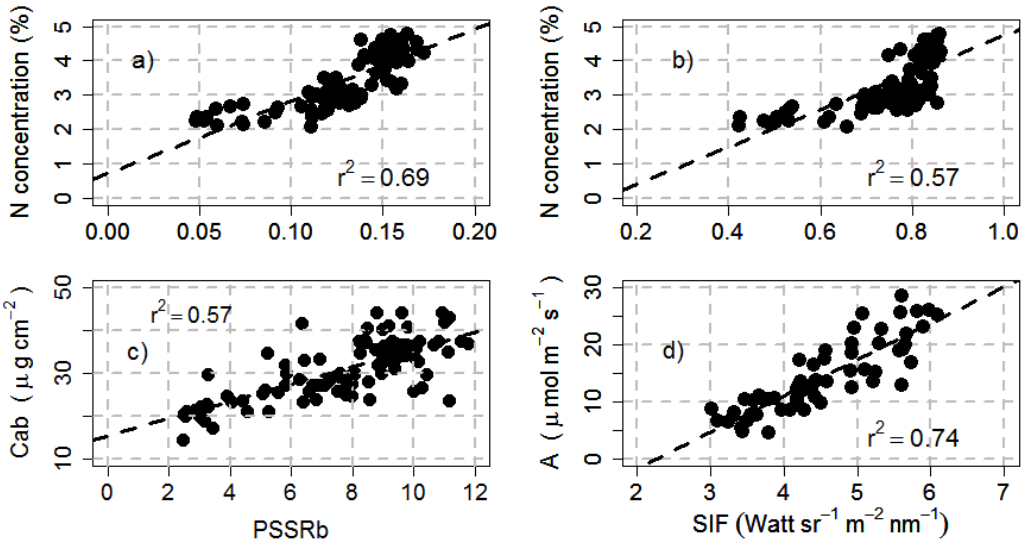


**Fig. 4**. Relationships between N concentration (in %) vs. NDNI (a) and NDVI (b), $C_{ab}$ vs. PSSRb (c) and A vs. airborne-quantified SIF (d). For all relationships the significance level was $p \leq 0.0005$.

### *3.3. Nitrogen content and plant traits estimated by model inversion*

The coefficient of determination ($r^2$) calculated between chlorophyll content ($C_{ab}$), water content ($C_w$) and dry matter content ($C_m$) estimated by PROSPECT-SAILH model inversion and leaf-level physiological measurements (nitrogen content, net assimilation rate and chlorophyll content) are shown in Table 6. These results correspond with the method proposed in Wang *et al.* (2015) that used biophysical parameters retrieved by model inversion to evaluate the retrieval of leaf N concentration. In the present study, $C_{ab}$ estimated by model inversion by steps correlated with N concentration ($r^2$=0.71; p-value ≤ 0.0005; Fig. 5a), field-measured leaf $C_{ab}$ ($r^2$=0.81; p-value ≤ 0.0005; Fig. 5b) and with the assimilation rate ($r^2$=0.59; p-value ≤ 0.0005; Fig. 5c). Using this model-inversion approach by steps, the relationship between estimated and measured $C_{ab}$ content adjusted well with the 1:1 line for the entire dataset (Fig. 5b), yielding a RMSE=2.04 µg·cm$^{-2}$ and

339 MAPE=5.44%. The two standard model-inversion methods (INV-1 and INV-2) displayed
340 quite different behavior; $C_{ab}$ was correctly estimated for plots with N concentration and $C_{ab}$
341 values that were higher than 3.5% and 30 $\mu g \cdot cm^{-2}$ respectively, while the retrievals failed
342 for the plots with nitrogen and $C_{ab}$ values below these (see outliers in Fig. 5b). The two
343 standard model inversion approaches thus yielded weaker results in their estimates of
344 nitrogen content (RMSE $\geq$ 6.33 $\mu g \cdot cm^{-2}$ and MAPE $\geq$ 17.68 %) than the model inversion
345 by steps.

**Table 6**. Coefficient of determination ($r^2$) between estimated leaf $C_{ab}$, $C_m$ and $C_w$ parameters by PROSPECT-SAILH model inversion by steps and by standard inversion methods (INV-1 and INV-2) vs. N concentration, leaf-measured $C_{ab}$ with SPAD, and net assimilation (A).

| | **N concentration** | **$C_{ab}$ (SPAD)** | **Net Assimilation (A)** |
|---|---|---|---|
| **Chlorophyll content a+b ($C_{ab}$)** | | | |
| **By step** | 0.71** | 0.81** | 0.59** |
| **INV-1** | 0.012 | 0.008 | 0.001 |
| **INV-2** | 0.004 | 0.002 | 0 |
| **Equivalent water thickness ($C_w$)** | | | |
| **By step** | 0.66** | 0.56** | 0.53** |
| **INV-1** | 0.017 | 0.008 | 0.008 |
| **INV-2** | 0.27** | 0.25** | 0.19* |
| **Dry-matter content ($C_m$)** | | | |
| **By step** | 0.23** | 0.1 | 0.18** |
| **INV-1** | 0.49** | 0.32** | 0.30** |
| **INV-2** | 0.38* | 0.24** | 0.23** |

** p-value < 0.0005; * p-value < 0.02

346 Leaf equivalent water thickness retrieval by model inversion was significantly related to N
347 concentration ($r^2$=0.66; p-value $\leq$ 0.0005), while dry matter content showed significant (yet
348 lower coefficients of determination than for $C_w$) yielding $r^2$=0.23 (step inversion method)
349 and $r^2$=0.49 (INV-1 method) (in both cases p-value $\leq$ 0.0005). In this case, the coefficient

of determination was significantly affected by outliers, inducing an artificial increase in the correlation coefficients for INV-1 as compared to the step inversion method. In summary, the three leaf biochemical parameters $C_{ab}$, $C_w$ and $C_m$ estimated by radiative transfer model inversion from the hyperspectral imagery were significantly related to leaf N concentration (p-value $\leq 0.0005$ in all three cases), but $C_{ab}$ and $C_w$ yielded higher relationship with N than $C_m$.

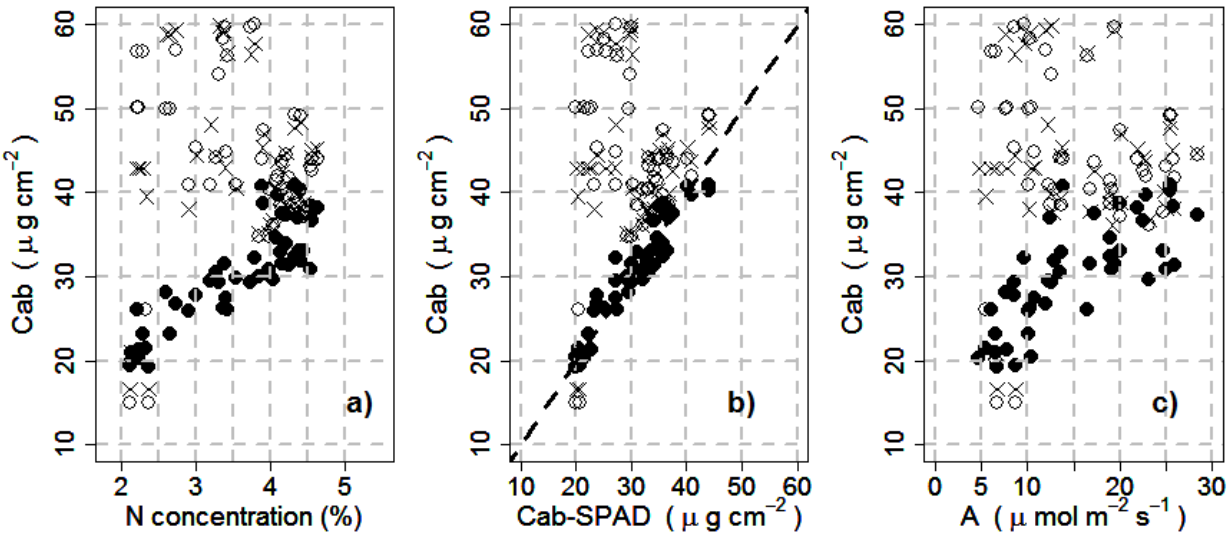


**Fig. 5**. Chlorophyll content ($C_{ab}$, µg·cm$^{-2}$) estimated by model inversions vs. N concentration (in %) (a), chlorophyll content derived from SPAD ($C_{ab}$-SPAD; µg·cm$^{-2}$) (b), and leaf assimilation rate (A, µmol·m$^{-2}$·s$^{-1}$) (c). Black points correspond to inversion by steps, black crosses using the INV-1 method and open black circles using the INV-2 model inversion method. The dashed line is the 1:1 line.

### *3.4. Leaf N estimation from the airborne hyperspectral imagery accounting for chlorophyll fluorescence*

The stepwise multiple regression and LOOCV methods built to estimate N concentration using the leaf biochemical constituents $C_{ab}$, $C_w$ and $C_m$ obtained by model inversion, were

assessed accounting for the contribution of adding chlorophyll fluorescence. The statistical models built using all input parameters, with and without including SIF as predictor of nitrogen are shown in Table 7. The homoscedasticity and the normal distribution requirements were satisfied and passed the statistical test (F-Test). According to the t-test, the regression coefficients for $C_{ab}$ and SIF were significant at the 5% significance level. In contrast, $C_m$ and $C_w$ parameters were non-significant in some of the regression models (see Table 7).

**Table 7.** Statistical tests for the validity of the regression models used to estimate N concentration.

| | **F-test** | | **Shapiro-Wilk** | **p-value (t-test)** | | | |
|---|---|---|---|---|---|---|---|
| | **p-value** | **W** | **p-value** | **$C_{ab}$** | **$C_w$** | **$C_m$** | **SIF** |
| **Without Fluorescence** | | | | | | | |
| **N=*f*($C_{ab}$)** | 2.4E-13 | 0.98 | 0.55 | 2.4E-13 | | | |
| **N=*f*($C_{ab}$,$C_w$)** | 2.9E-16 | 0.98 | 0.64 | 6.2E-06 | 0.0003 | | |
| **N=*f*($C_{ab}$,$C_m$)** | 7.5E-17 | 0.98 | 0.46 | 7.6E-14 | | 8.2E-5 | |
| **N=*f*($C_{ab}$,$C_w$,$C_m$)** | 6.4E-17 | 0.98 | ≥0.05 | 8.7E-06 | 0.5911 | 0.0906 | |
| **With Fluorescence** | | | | | | | |
| **N=*f*($C_{ab}$, SIF)** | 8.2E-27 | 0.97 | 0.35 | 7.8E-10 | 1.1E-14 | | |
| **N=*f*($C_{ab}$,$C_w$,SIF)** | 1.4E-28 | 0.96 | 0.17 | 1.0E-06 | 0.0059 | | 2.7E-13 |
| **N=*f*($C_{ab}$,$C_m$,SIF)** | 1.1E-27 | 0.97 | 0.23 | 1.9E-10 | | 0.0519 | 7.2E-12 |
| **N=*f*($C_{ab}$,$C_w$,$C_m$,SIF)** | 1.2E-28 | 0.97 | 0.2 | 0.0013 | 0.0429 | 0.5395 | 1.8E-12 |

The ability of each model to predict N concentration was assessed using the LOOCV scores described earlier, showing the results in Table 8. Based on these statistical scores, the multiple linear regression models using SIF as predictive variable considerably improved the accuracy of N estimation ($r^2_{LOOCV} \geq 0.92$; $MAE_{LOOCV} \leq 0.19$ and $RMSE_{LOOCV} \leq 0.23$). As a comparison, regression models without including fluorescence (SIF) reached significantly lower predictive power ($r^2_{LOOCV} \leq 0.77$; $MAE_{LOOCV} \geq 0.33$ and $RMSE_{LOOCV}$

373 ≥ 0.40). The contribution of each variable is shown by standardized coefficients ($\beta_0$; Table
374 8). These results show that in models that include SIF as predictor, its contribution to the
375 retrieval of N was higher than the rest of the predictors, being almost double than the
376 contribution of $C_{ab}$. In the models that did not use SIF as predictor, the estimated $C_{ab}$ by
377 model inversion contributed the highest to N estimation.

| **Regression Models** | **$r^2$** | **RMSE** | **MAE** | **MAPE** | **Standard. coefficients (β0)** | | | |
|---|---|---|---|---|---|---|---|---|
| | | | | | **$C_{ab}$** | **$C_w$** | **$C_m$** | **SIF** |
| **Without Fluorescence** | | | | | | | | |
| **N=*f*($C_{ab}$)** | 0.68 | 0.47 | 0.39 | 12.0% | 0.84 | … | …. | … |
| **N=*f*($C_{ab}$, $C_w$)** | 0.74 | 0.41 | 0.34 | 9.9% | 0.54 | 0.41 | … | … |
| **N=*f*($C_{ab}$, $C_m$)** | 0.77 | 0.40 | 0.33 | 9.7% | 0.77 | … | -0.31 | … |
| **N=*f*($C_{ab}$, $C_w$, $C_m$)** | 0.75 | 0.41 | 0.34 | 10.0% | 0.70 | 0.11 | -0.24 | … |
| **With Fluorescence** | | | | | | | | |
| **N=*f*($C_{ab}$, SIF)** | 0.92 | 0.23 | 0.19 | 5.9% | 0.43 | … | … | 0.63 |
| **N=*f*($C_{ab}$, $C_w$, SIF)** | 0.92 | 0.22 | 0.18 | 5.6% | 0.34 | 0.17 | … | 0.57 |
| **N=*f*($C_{ab}$, $C_m$, SIF)** | 0.92 | 0.23 | 0.19 | 5.9% | 0.44 | … | -0.10 | 0.57 |
| **N=*f*($C_{ab}$, $C_w$, $C_m$, SIF)** | 0.93 | 0.20 | 0.18 | 5.5% | 0.30 | 0.23 | 0.05 | 0.58 |

**Table 8**. Performance of the regression models built to estimate N concentration using $r^2$, RMSE, ME, MAE, MAPE and standardized coefficients as performance indicators.

378 According to $r^2$, RMSE, MAE and MAPE, the most accurate estimation was achieved by
379 the regression model when the predictors were $C_{ab}$, $C_w$, $C_m$ and SIF, yielding
380 $r^2_{LOOCV} = 0.93$, $RMSE_{LOOCV} = 0.20$, $MAE_{LOOCV} = 0.18$ and the lowest MAPE (Table 8).
381 Nevertheless, the rest of models with less number of parameters (therefore simpler)
382 obtained accuracies only marginally lower (e.g. $r^2$=0.93 & RMSE=0.20 for the most
383 complex model using $C_{ab}$, $C_w$, $C_m$ and SIF as compared to $r^2$=0.92 & RMSE=0.23 for the
384 model using $C_{ab}$ and SIF). Figure 6 shows the scatter plots between the measured and

385 predicted N concentrationusing the model without (top plots) and with SIF as predictor
386 (bottom plots). The models using SIF showed lower RMSE and better performance than the
387 rest of the models that did not employ fluorescence as predictor.

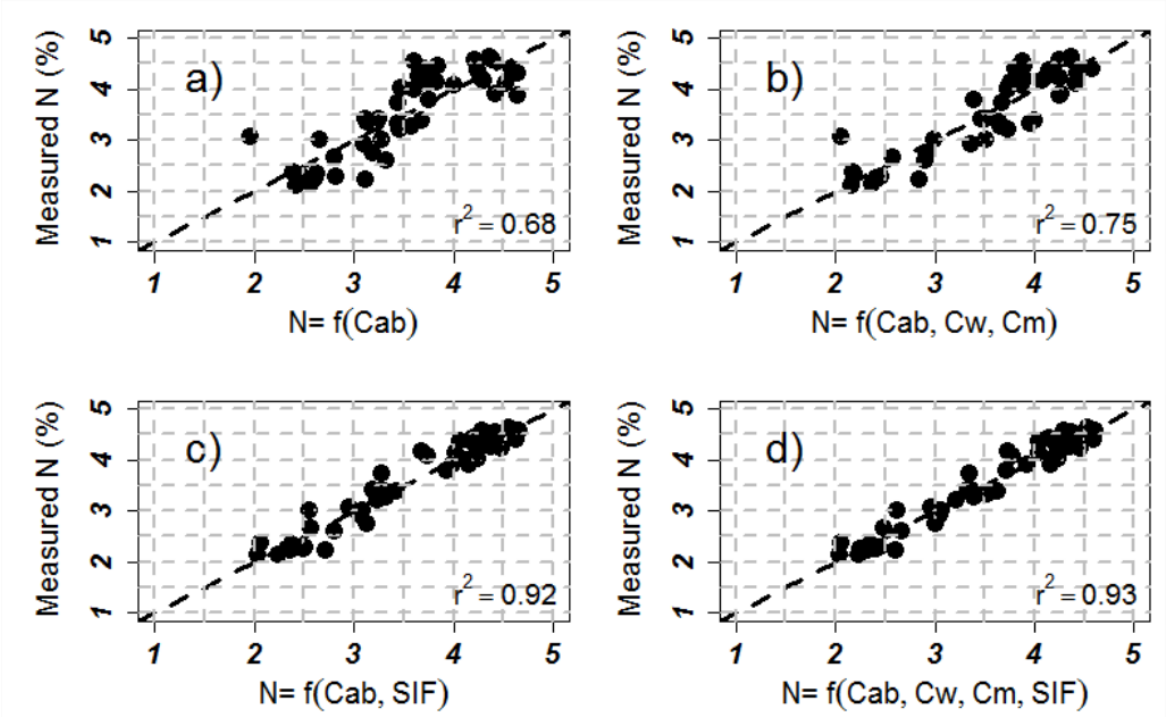


**Fig. 6**. Measured vs. estimated N concentration using the best regression LOOCV models without fluorescence (a,b) and with fluorescence (c,d) as a function of $C_{ab}$ (a), $C_{ab}$, $C_w$ and $C_m$ (b), $C_{ab}$ and SIF (c) and $C_{ab}$, $C_w$, $C_m$ and SIF (d). The dashed line is the 1:1 line.

388 Based on these results, the proposed models combining leaf biochemical constituents with
389 and without SIF were evaluated as predictors for N concentration separately for rainfed and
390 irrigated conditions. All models showed greater accuracies in predicting N concentration
391 under rainfed (stress) conditions than under irrigated (non-water stress) conditions (e.g. best
392 model performance yielded $r^2$=0.93 (rainfed) vs. $r^2$=0.88; (irrigated) (Table 9). As Figure 7
393 shows, the plots were aligned over the 1:1 line for both cases of rainfed (Fig. 7a) and
394 irrigated conditions (Fig. 7b). Under rainfed conditions, the models with SIF as predictor

yielded significantly higher scores ($r^2 \geq 0.89$, RMSE $\leq 0.26$ and MAPE $\leq 6.8$ %) than models without SIF as predictor ($r^2 \geq 0.78$, RMSE $\leq 0.37$ and MAPE $\leq 9.46$ %).

**Table 9**. Statistics for $r^2$, RMSE, ME, MAE, MPE and MAPE between measured and predicted N concentration under rainfed and irrigated conditions.

| | $r^2$ | RMSE | MAE | MPE | MAPE |
|---|---|---|---|---|---|
| **Rainfed conditions** | | | | | |
| **Without Fluorescence** | | | | | |
| **N = *f*($C_{ab}$)** | 0.78 | 0.37 | 0.29 | -1.44% | 9.46% |
| **N = *f*($C_{ab}$, $C_m$)** | 0.81 | 0.34 | 0.27 | -1.12% | 8.50% |
| **N = *f*($C_{ab}$, $C_w$)** | 0.86 | 0.36 | 0.23 | -0.92% | 7.54% |
| **N = *f*($C_{ab}$, $C_w$, $C_m$)** | 0.86 | 0.29 | 0.23 | -0.84% | 7.24% |
| **With Fluorescence** | | | | | |
| **N=*f*($C_{ab}$, SIF)** | 0.89 | 0.26 | 0.21 | -0.65% | 6.89% |
| **N = *f*($C_{ab}$, $C_m$, SIF)** | 0.89 | 0.26 | 0.22 | -0.64% | 6.86% |
| **N = *f*($C_{ab}$, $C_w$, SIF)** | 0.92 | 0.23 | 0.18 | -0.45% | 5.68% |
| **N = *f*($C_{ab}$, $C_w$, $C_m$, SIF)** | 0.93 | 0.22 | 0.18 | -0.45% | 5.65% |
| **Irrigated conditions** | | | | | |
| **Without Fluorescence** | | | | | |
| **N = *f*($C_{ab}$)** | 0.48 | 0.51 | 0.44 | -2.03% | 12.56% |
| **N = *f*($C_{ab}$, $C_m$)** | 0.59 | 0.45 | 0.37 | -1.65% | 10.50% |
| **N = *f*($C_{ab}$, $C_w$)** | 0.76 | 0.35 | 0.29 | -0.89% | 8.05% |
| **N = *f*($C_{ab}$, $C_w$, $C_m$)** | 0.77 | 0.34 | 0.28 | -0.85% | 7.68% |
| **With Fluorescence** | | | | | |
| **N=*f*($C_{ab}$, SIF)** | 0.65 | 0.42 | 0.36 | -1.41% | 10.6% |
| **N = *f*($C_{ab}$, $C_m$, SIF)** | 0.77 | 0.34 | 0.27 | -0.93% | 7.89% |
| **N = *f*($C_{ab}$, $C_w$, SIF)** | 0.84 | 0.28 | 0.34 | -0.58% | 6.77% |
| **N = *f*($C_{ab}$, $C_w$, $C_m$, SIF)** | 0.88 | 0.25 | 0.20 | -0.47% | 5.63% |

Under irrigated conditions, the models that used SIF as predictor also showed the best performance. The model built with $C_{ab}$ and SIF displayed better accuracy in predicting nitrogen concentration ($r^2 = 0.65$, RMSE = 0.42 and MAPE $\leq 10.6$ %) than the model with $C_{ab}$ only ($r^2 = 0.48$, RMSE = 0.51 and MAPE $\leq 12.56$ %), indicating that the contribution of SIF was highly significant under both irrigated and non-irrigated conditions.

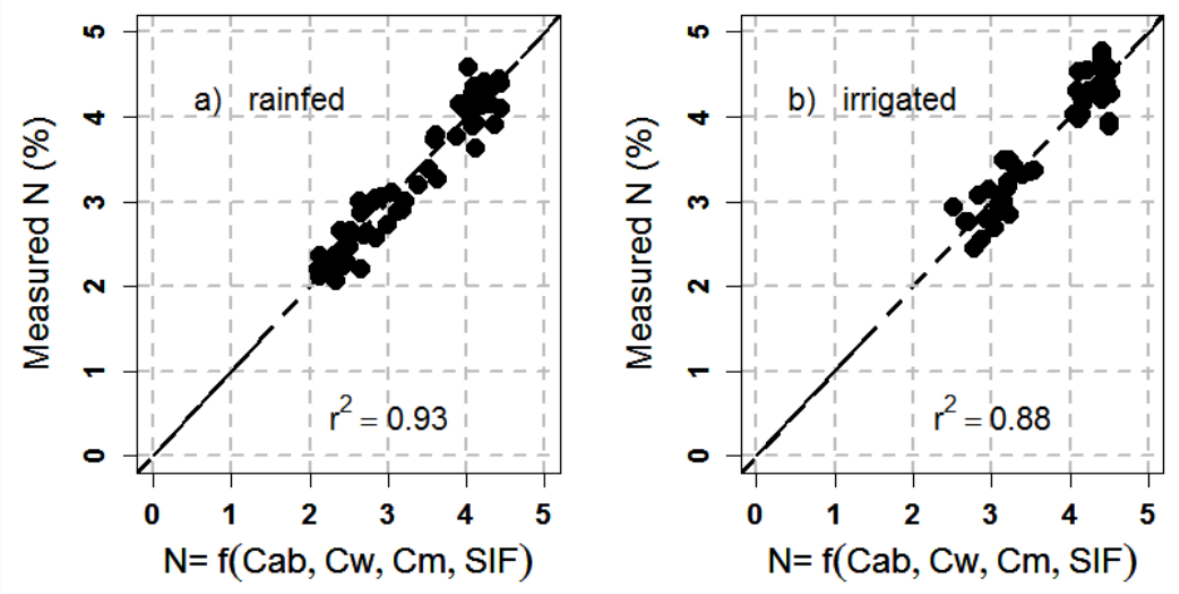


**Fig. 7**. Measured vs. estimated N concentration for rainfed (a) and irrigated conditions (b) using the model built with $C_{ab}$, $C_m$ and $C_w$ biochemical constituents (estimated by model inversion) including fluorescence. The solid line is the 1:1 line.

These modelling methods enabled the quantification of N concentration from the hyperspectral imagery to show its spatial distribution in the context of precision agriculture and plant phenotyping experiments. Figure 8 shows the spatial distribution of N concentration using $C_{ab}$, $C_w$, $C_m$ and SIF as predictors (Figure 8a) over plots under rainfed (Figure 8b) and irrigated conditions (Figure 8c) at the SA field site during the 2016 campaign. Higher values of nitrogen concentration (blue color) from the rainfed plots indicate a better physiological status, while low N values (red color) indicate stress levels as consequence of the rainfed conditions. In comparison with irrigated conditions, the N map clearly showed the lower values obtained in the rainfed fields, with average values of 3.1± 0.18%; under irrigated conditions the average N concentration was higher (4.2± 0.3%). This methodology enables an operational quantification of canopy N concentration

414 at the field level using high resolution hyperspectral remote sensing imagery and radiative-
415 transfer model inversion methods.

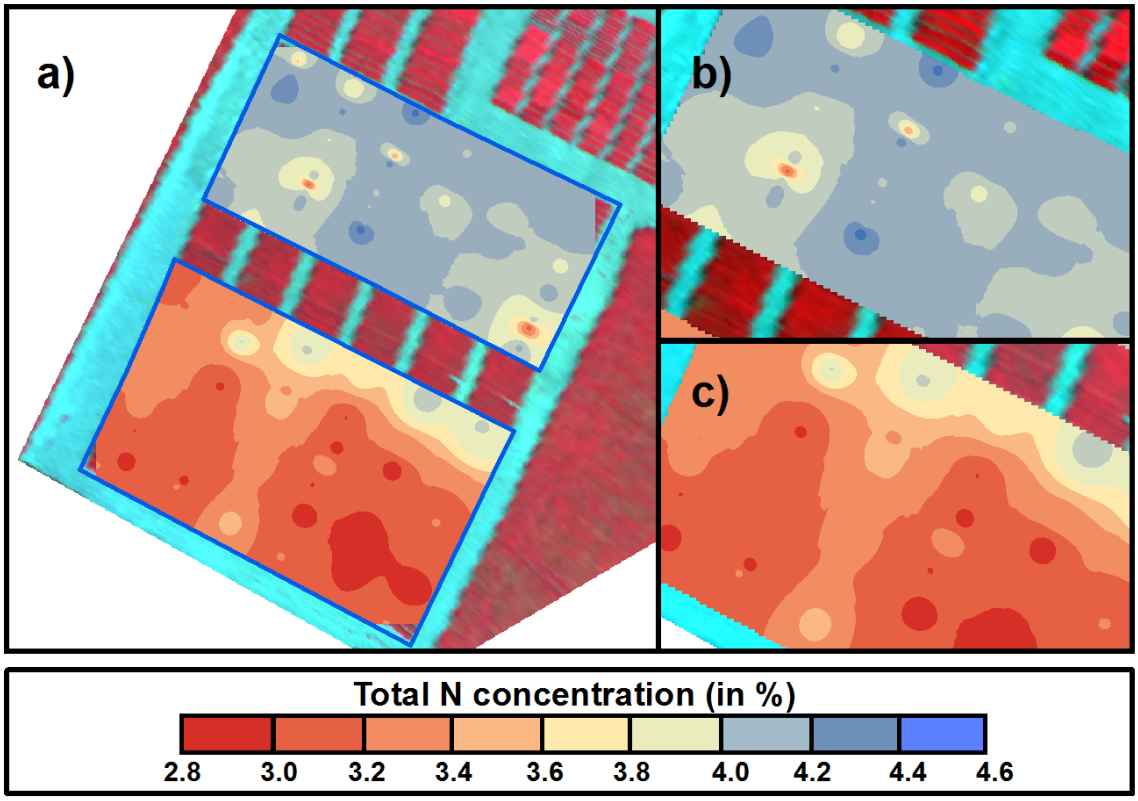


**Fig. 8**. Map showing the spatial distribution of N concentration estimated using the model built with chlorophyll a+b ($C_{ab}$), water content ($C_w$), dry matter content ($C_m$) and solar induced chlorophyll fluorescence (SIF) estimated from hyperspectral imagery (a) and used as predictors under irrigated (b) and rainfed (c) conditions at SA field site during the 2016 airborne campaign.

416

417 **4. Discussion**

418 Several studies have focused on the estimation of canopy N concentration using remote
419 sensing techniques. The main problem encountered is that N does not absorb radiation with
420 distinct features to enable its direct quantification with reflectance data. Instead, proxies
421 physiologically related to N which are potentially retrievable from remote sensing spectra

422 are proposed as the only feasible way of detecting nitrogen levels under nutrient-deficiency
423 conditions. An example is the widely used SPAD meter, a hand held instrument that
424 measures chlorophyll content and generally accepted to track N concentration at the leaf
425 level (Ravier *et al*., 2017). Most of the studies that assess the retrieval of N through non-
426 destructive methods have been traditionally based on empirical models with spectral
427 indices (i.e. spectral proxies) calculated from the visible (VIS) and near-infrared (NIR)
428 regions (Clevers and Kooistra, 2012; Li *et al*., 2014), while only a few studies focused on
429 radiative transfer model inversions and the relationships between retrieved parameters (i.e.
430 biophysical parameters and biochemical constituents as proxies) and nitrogen (Thorp *et al*.,
431 2012; Wang *et al*., 2015). The present study evaluated these standard hyperspectral remote
432 sensing techniques for the estimation of N concentration using narrow-band indices
433 combining the VNIR and the SWIR region, but focusing on the potential contribution of a
434 new indicator such as the radiance-based fluorescence SIF for improving the performance
435 of N estimation. According to the results obtained by the regression models built with $C_{ab}$,
436 $C_w$, $C_m$ and SIF from the stepwise multiple regression and LOOCV methods, the solar
437 induced chlorophyll fluorescence quantified from the hyperspectral imagery significantly
438 increased the performance for the estimation of N. This result confirms the findings of
439 other studies that suggested a close link between fluorescence emission and nitrogen (Corp
440 *et al*., 2003; Schächtl *et al*., 2005; Cendrero-Mateo *et al*., 2016). The contribution of SIF to
441 predict N concentration was higher than that of $C_{ab}$ and leaf biochemical parameters such as
442 dry matter and equivalent water thickness. In fact, models containing fluorescence emission
443 among their predictors produced the most reliable nitrogen estimation when compared to
444 models without SIF. The results indicated that SIF retrieval by the FLD method from high
445 resolution hyperspectral imagery demonstrated its value for monitoring N concentration

446 under both rainfed and irrigated conditions in the context of precision agriculture and plant
447 phenotyping studies. The solar induced chlorophyll fluorescence provides a potential new
448 tool to estimate canopy N concentration, due to their close link with photosynthetic
449 parameters such as the maximum rate of carboxilation and with plant functioning. These
450 results agree with recent studies that showed the ability of such methods to evaluate crop
451 physiological status under conditions of water stress, compared to hyperspectral narrow-
452 band indices (Herrmann *et al*., 2010; Ranjan *et al*., 2012; Gonzalez-Dugo *et al*., 2015;
453 Zarco-Tejada *et al*., 2016). This study also demonstrates that the biophysical parameters
454 retrieved from a radiative transfer model at canopy scale are needed for better N
455 concentration estimation due to the more robust quantification of the parameters as
456 compared to single narrow-band hyperspectral indices. This agrees with Wang *et al*. (2015)
457 who demonstrated that the combination of biophysical parameters (leaf chlorophyll, dry
458 matter and water content) retrieved via PROSPECT model inversion provided a reliable
459 tool to estimate N at leaf scale. They found a higher correlation between leaf nitrogen
460 content and dry matter and water content than with chlorophyll. Our results indicate that, in
461 the absence of chlorophyll fluorescence as predictor, chlorophyll a+b was the parameter
462 most related with nitrogen. This result is in agreement with other studies that indicate that
463 the chlorophyll is the most widely used proxy for N estimation (Herrmann *et al*., 2010;
464 Homolová *et al*., 2013). In this regard, this study displayed that $C_w$ and $C_m$ contributions for
465 predicting nitrogen concentration were lower than $C_{ab}$ and SIF in both rainfed and irrigated
466 conditions. However, it was observed that under irrigated conditions the models showed
467 lower accuracy at predicting N concentration, especially when Cab was the only predictor.
468 Under the conditions of this experiment, the lower performance obtained for irrigated vs.
469 rainfed conditions was likely due to the smaller range of variability found for the predictors

in the irrigated than in the rainfed plots. The results of this study showed that the contribution of SIF (which can be also derived from VNIR cameras) is superior than the contribution of the NIR-SWIR camera used here to estimate dry matter and equivalent water thickness. Considering the cost, complexity of operation, and the lower resolution generally obtained by SWIR cameras, the interest of retrieving SIF and chlorophyll content from a single VNIR camera outperforms the SWIR under the conditions and objectives of the present study.

This work also demonstrates that the model inversion by steps yields more reliable retrievals than traditional inversions, which used the entire VNIR up to 1700 nm region to retrieve all parameters simultaneously. This result shows that model inversions conducted by steps reduced the ill-posed inverse problems (Combal *et al*., 2003; Wang *et al*., 2007; Yebra and Chuvieco, 2009; Li and Wang, 2011) and improves the parameter retrievals. Our results also confirm findings by Li and Wang (2011) regarding this issue.

Another important result obtained in this study shows that the regression models built with parameters obtained by model-inversion yielded superior results than simple linear models based on spectral indices (Herrmann *et al*., 2010; Pimstein *et al*., 2011; Bao *et al*., 2013; Mahajan *et al*., 2014; Gnyp *et al*., 2014). This conclusion was true even when using narrow-band indices centered at 1510 and 850 nm, which are highly correlated with N concentration. Regarding hyperspectral indices, our results confirmed findings reported by Herrmann *et al*. (2010) that the use of the SWIR domain significantly improved the estimation of nitrogen concentration when compared to the visible and near-infrared region of the spectrum. In our case, the use of the SWIR spectral range to determine NIs provided

494 better quantification of N concentration than when only the VNIR region was used, in
495 particular when using indices from bands centered at 1510 nm (Herrmann *et al*., 2010;
496 Serrano *et al*., 2002). Among all indices, the NIs that combined 1510 nm and VNIR bands
497 yielded the highest agreement with N concentration (e.g. $r^2$=0.69 for $MCARI_{1510}$ and
498 $r^2$=0.65 for $NI_{1850/1510}$). However, these simple relationships obtained between N
499 concentration and chlorophyll indices are affected by structure and the underlying soil. By
500 contrast, the structural indices (e.g. NDVI) tend to saturate their values under dense
501 canopies and with high nitrogen levels (Fig. 4b). Nevertheless, none of the hyperspectral
502 index combinations outperformed the results obtained by model inversion when adding
503 fluorescence (i.e. $C_{ab}$+$C_m$+$C_w$+SIF), which was by far the best model for N estimation.
504
505 An additional important topic is that the methodology used here for the airborne retrieval of
506 chlorophyll fluorescence from radiance imagery is based on the work presented in previous
507 studies (e.g.: Damm *et al*., 2015; Zarco-Tejada *et al*., 2016), confirming that the use of
508 hyperspectral imagery acquired at broader spectral bands (i.e. with FWHM 2-7 nm) retains
509 sufficient chlorophyll fluorescence signal to yield the most significant relationships against
510 field-measured assimilation rates among all other image-derived indicators.
511
512 An issue observed in this work is the potential limitations of the plot sizes normally used by
513 plant breeders during their experimental designs. The plot dimension should be compatible
514 with the spatial resolution of the imagery acquired by remote sensing. When the plots are
515 too small, soil and background effects may play a critical role due to the mixing of the
516 different components (i.e. soil and shadows) with the vegetation. This issue is important in
517 the case in of the coarser resolution generally obtained by SWIR cameras. New sensors

carried on board drones and low-altitude manned aircraft can potentially obtain high- and ultra-high resolutions, which are compatible with the standard phenotyping and plant breeding experiments. Nevertheless, plant breeding experimental design should be compatible with the spatial resolutions of the remote sensing sensors to be flown over the study sites. In this way, a line of at least 1/2 to 1 pixel as edge around the center of the plot is recommended.

## 5. Conclusions

The present study demonstrates that the airborne-quantified solar induced chlorophyll fluorescence (SIF) is a critical predictor for the estimation of N concentration under semi-arid and arid conditions when combined with chlorophyll a+b content and leaf parameters dry matter ($C_m$) and equivalent water thickness ($C_w$) plant traits retrieved by radiative transfer model inversion. When the models were built with airborne-quantified SIF, N estimation performance improved under both rainfed (water-stress) and irrigated conditions. Additionally, the models that combined SIF and chlorophyll a+b content performed better than standard empirical methods based on simple linear relationships with narrow-band hyperspectral indices. In addition, this work demonstrates that SWIR-based indices centered at 1510 nm yield more reliable agreements with N concentration ($r^2$=0.69) than traditional chlorophyll indices (TCARI/OSAVI $r^2$=0.45) proposed as proxy for N quantification.

## Acknowledgments

The authors gratefully acknowledge the financial support of the Spanish Ministry of Science and Education (MEC) for projects AGL2012-40053-C03-01, and AGL2012-35196 and the Junta de Andalucia for projects P12-AGR-2521 and P12-AGR-0482. Dr Ignacio Solis Martel from Agrovegetal S.A. is gratefully acknowledged for facilitating access and sampling of their experimental farm. D. Notario, A. Vera, A. Hornero, R. Romero and R. Mérida-Garcia are also thanked for their technical support during the field and airborne campaigns.

## References

Bao, Y., Xu, K., Min, J., Xu, J., 2013. Estimating wheat shoot nitrogen content at vegetative stage from in situ hyperspectral measurements. Crop Sci. 53, 2063–2071. doi:10.2135/cropsci2013.01.0012

Baret, F., Fourty, T., 1997. Estimation of leaf water content and specific leaf weight from reflectance and transmittance measurements. Agronomie 17, 455–464. doi:10.1051/agro:19970903

Baret, F., Jacquemoud, S., Guyot, G., Leprieur, C., 1992. Modeled analysis of the biophysical nature of spectral shifts and comparison with information content of broad bands. Remote Sens. Environ. 41, 133–142. doi:10.1016/0034-4257(92)90073-S

Berni, J., Zarco-Tejada, P.J., Suarez, L., Fereres, E., 2009. Thermal and Narrowband Multispectral Remote Sensing for Vegetation Monitoring From an Unmanned Aerial Vehicle. IEEE Trans. Geosci. Remote Sens. 47, 722–738.

563 doi:10.1109/TGRS.2008.2010457

564 Blackburn, G.A., 1998. Spectral indices for estimating photosynthetic pigment
565 concentrations : a test using senescent tree leaves. Int. J. Remote Sens. 19, 657–675.
566 doi:10.1080/014311698215919

567 Calderón, R., Navas-Cortés, J.A., Lucena, C., Zarco-Tejada, P.J., 2013. High-resolution
568 airborne hyperspectral and thermal imagery for early detection of Verticillium wilt of olive
569 using fluorescence, temperature and narrow-band spectral indices. Remote Sens. Environ.
570 139, 231–245. doi:10.1016/j.rse.2013.07.031

571 Calderón, R., Navas-Cortés, J.A., Zarco-Tejada, P.J., 2015. Early detection and
572 quantification of Verticillium Wilt in olive using hyperspectral and thermal imagery over
573 large areas. Remote Sens. 7, 5584–5610. doi:10.3390/rs70505584

574 Cendrero-Mateo, M.P., Moran, M.S., Papuga, S.A., Thorp, K.R., Alonso, L., Moreno, J.,
575 Ponce-Campos, G., Rascher, U., Wang, G., 2016. Plant chlorophyll fluorescence: Active
576 and passive measurements at canopy and leaf scales with different nitrogen treatments. J.
577 Exp. Bot. 67, 275–286. doi:10.1093/jxb/erv456

578 Chen, P., Haboudane, D., Tremblay, N., Wang, J., Vigneault, P., Li, B., 2010. New spectral
579 indicator assessing the efficiency of crop nitrogen treatment in corn and wheat. Remote
580 Sens. Environ. 114, 1987–1997. doi:10.1016/j.rse.2010.04.006

581 Clevers, J.G.P.W., Kooistra, L., 2012. Using hyperspectral remote sensing data for
582 retrieving canopy chlorophyll and nitrogen content. IEEE J. Sel. Top. Appl. Earth Obs.
583 Remote Sens. 5, 574–583. doi:10.1109/JSTARS.2011.2176468

584 Combal, B., Baret, F., Weiss, M., Trubuil, A., Macé, D., Pragnère, A., Myneni, R.,
585 Knyazikhin, Y., Wang, L., 2003. Retrieval of canopy biophysical variables from
586 bidirectional reflectance using prior information to solve the ill-posed inverse problem.
587 Remote Sens. Environ. 84, 1–15. doi:10.1016/S0034-4257(02)00035-4

588 Corp, L.A., McMurtrey, J.E., Middleton, E.M., Mulchi, C.L., Chappelle, E.W., Daughtry,
589 C.S.T., 2003. Fluorescence sensing systems: In vivo detection of biophysical variations in
590 field corn due to nitrogen supply. Remote Sens. Environ. 86, 470–479. doi:10.1016/S0034-
591 4257(03)00125-1

592 Croft, H., Chen, J.M., Luo, X., Bartlett, P., Chen, B., Staebler, R.M., 2017. Leaf
593 chlorophyll content as a proxy for leaf photosynthetic capacity. Glob. Chang. Biol. 23,
594 3513–3524. doi:10.1111/gcb.13599

595 Damm, A., Erler, A., Hillen, W., Meroni, M., Schaepman, M.E., Verhoef, W., Rascher, U.,
596 2011. Modeling the impact of spectral sensor configurations on the FLD retrieval accuracy
597 of sun-induced chlorophyll fluorescence. Remote Sens. Environ. 115, 1882–1892.
598 https://doi.org/10.1016/j.rse.2011.03.011

599 Damm, A., Guanter, L., Paul-Limoges, E., van der Tol, C., Hueni, A., Buchmann, N.,
600 Eugster, W., Ammann, C., Schaepman, M.E., 2015. Far-red sun-induced chlorophyll
601 fluorescence shows ecosystem-specific relationships to gross primary production: An
602 assessment based on observational and modeling approaches. Remote Sens. Environ. 166,
603 91–105. doi:10.1016/j.rse.2015.06.004

604 Daughtry, C., 2000. Estimating Corn Leaf Chlorophyll Concentration from Leaf and
605 Canopy Reflectance. Remote Sens. Environ. 74, 229–239. doi:10.1016/S0034-

606 4257(00)00113-9

607 Eitel, J.U.H., Long, D.S., Gessler, P.E., Smith, A.M.S., 2007. Using in-situ measurements
608 to evaluate the new RapidEye$^{TM}$ satellite series for prediction of wheat nitrogen status. Int.
609 J. Remote Sens. 28, 4183–4190. doi:10.1080/01431160701422213

610 Feret, J.B., François, C., Asner, G.P., Gitelson, A.A., Martin, R.E., Bidel, L.P.R., Ustin,
611 S.L., le Maire, G., Jacquemoud, S., 2008. PROSPECT-4 and 5: Advances in the leaf optical
612 properties model separating photosynthetic pigments. Remote Sens. Environ. 112, 3030–
613 3043. doi:10.1016/j.rse.2008.02.012

614 Ferwerda, J.G., Skidmore, A.K., Mutanga, O., 2005. Nitrogen detection with hyperspectral
615 normalized ratio indices across multiple plant species. Int. J. Remote Sens. 26, 4083–4095.
616 doi:10.1080/01431160500181044

617 Fourty, T., Baret, F., Jacquemoud, S., Schmuck, G., Verdebout, J., 1996. Leaf optical
618 properties with explicit description of its biochemical composition: Direct and inverse
619 problems. Remote Sens. Environ. 56, 104–117. doi:10.1016/0034-4257(95)00234-0

620 Genty, B., Briantais, J.M., Baker, N.R., 1989. The relationship between the quantum yield
621 of photosynthetic electron transport and quenching of chlorophyll fluorescence. Biochim.
622 Biophys. Acta - Gen. Subj. 990, 87–92. doi:10.1016/S0304-4165(89)80016-9

623 Gitelson, A. A., Merzlyak, M.N., 1997. Remote estimation of chlorophyll content in higher
624 plant leaves. Int. J. Remote Sens. 18, 2691–2697. doi:10.1080/014311697217558

625 Gnyp, M.L., Bareth, G., Li, F., Lenz-Wiedemann, V.I.S., Koppe, W., Miao, Y., Hennig,
626 S.D., Jia, L., Laudien, R., Chen, X., Zhang, F., 2014. Development and implementation of a

627 multiscale biomass model using hyperspectral vegetation indices for winter wheat in the
628 North China Plain. Int. J. Appl. Earth Obs. Geoinf. 33, 232–242.
629 doi:10.1016/j.jag.2014.05.006

630 Gonzalez-Dugo, V., Durand, J.-L., Gastal, F., 2010. Water deficit and nitrogen nutrition of
631 crops. A review. Agron. Sustain. Dev. 30, 529–544. doi:10.1051/agro/2009059

632 Gonzalez-Dugo, V., Hernandez, P., Solis, I., Zarco-Tejada, P.J., 2015. Using high-
633 resolution hyperspectral and thermal airborne imagery to assess physiological condition in
634 the context of wheat phenotyping. Remote Sens. 7, 13586–13605. doi:10.3390/rs71013586

635 Gueymard, C., 1995. SMARTS, a simple model of the atmospheric radiative transfer of
636 sunshine: Algorithms and performance assessment. Technical report no. FSEC-PF-270-95.
637 Cocoa, FL: Florida Solar Energy Center.

638 Gueymard, C.A., Myers, D., Emery, K., 2002. Proposed reference irradiance spectra for
639 solar energy systems testing. Sol. Energy 73, 443–467. doi:10.1016/S0038-
640 092X(03)00005-7

641 Haboudane, D., Miller, J.R., Pattey, E., Zarco-Tejada, P.J., Strachan, I.B., 2004.
642 Hyperspectral vegetation indices and novel algorithms for predicting green LAI of crop
643 canopies: Modeling and validation in the context of precision agriculture. Remote Sens.
644 Environ. 90, 337–352. doi:10.1016/j.rse.2003.12.013

645 Haboudane, D., Miller, J.R., Tremblay, N., Zarco-Tejada, P.J., Dextraze, L., 2002.
646 Integrated narrow-band vegetation indices for prediction of crop chlorophyll content for
647 application to precision agriculture. Remote Sens. Environ. 81, 416–426.

doi:10.1016/S0034-4257(02)00018-4

Herrmann, I., Karnieli, A., Bonfil, D.J., Cohen, Y., Alchanatis, V., 2010. SWIR-based spectral indices for assessing nitrogen content in potato fields. Int. J. Remote Sens. 31, 5127–5143. doi:10.1080/01431160903283892

Homolová, L., Malenovský, Z., Clevers, J.G.P.W., García-Santos, G., Schaepman, M.E., 2013. Review of optical-based remote sensing for plant trait mapping. Ecol. Complex. 15, 1–16. doi:10.1016/j.ecocom.2013.06.003

Houborg, R., Cescatti, A., Migliavacca, M., Kustas, W.P., 2013. Satellite retrievals of leaf chlorophyll and photosynthetic capacity for improved modeling of GPP. Agric. For. Meteorol. 117, 10–23. doi:10.1016/j.agrformet.2013.04.006

Jacquemoud, S., Baret, F., 1990. PROSPECT: A model of leaf optical properties spectra. Remote Sens. Environ. 34, 75–91. doi:10.1016/0034-4257(90)90100-Z

Jacquemoud, S., Ustin, S.L., Verdebout, J., Schmuck, G., Andreoli, G., Hosgood, B., 1996. Estimating leaf biochemistry using the PROSPECT leaf optical properties model. Remote Sens. Environ. 56, 194–202. doi:10.1016/0034-4257(95)00238-3

Jacquemoud, S., Verhoef, W., Baret, F., Bacour, C., Zarco-Tejada, P.J., Asner, G.P., François, C., Ustin, S.L., 2009. PROSPECT + SAIL models: A review of use for vegetation characterization. Remote Sens. Environ. 113, S56–S66. doi:10.1016/j.rse.2008.01.026

Jin, X., Yang, G., Tan, C., Zhao, C., 2015. Effects of nitrogen stress on the photosynthetic CO2 assimilation, chlorophyll fluorescence, and sugar-nitrogen ratio in corn. Sci. Rep. 5, 9311. doi:10.1038/srep09311

669 Khamis, S., Lamaze, T., Lemoine, Y., Foyer, C., 1990. Adaptation of the Photosynthetic
670 Apparatus in Maize Leaves as a Result of Nitrogen Limitation : Relationships between
671 Electron Transport and Carbon Assimilation. Plant Physiol. 94, 1436–1443.
672 doi:10.1104/pp.94.3.1436

673 Kjeldahl, J., 1883. Neue Methode zur Bestimmung des Stickstoffs in organischen. J. Anal.
674 Chem. 366–382. doi:10.1007/BF01338151

675 Kokaly, R., 1999. Spectroscopic Determination of Leaf Biochemistry Using Band-Depth
676 Analysis of Absorption Features and Stepwise Multiple Linear Regression. Remote Sens.
677 Environ. 67, 267–287. doi:10.1016/S0034-4257(98)00084-4

678 Lemaire, G., Jeuffroy, M.-H., Gastal, F., 2008. Diagnosis tool for plant and crop N status in
679 vegetative stage: Theory and practices for crop N management. Eur. J. Agron. 28, 614–624.
680 doi:10.1016/j.eja.2008.01.005

681 Li, F., Mistele, B., Hu, Y., Chen, X., Schmidhalter, U., 2014. Reflectance estimation of
682 canopy nitrogen content in winter wheat using optimised hyperspectral spectral indices and
683 partial least squares regression. Eur. J. Agron. 52, 198–209. doi:10.1016/j.eja.2013.09.006

684 Li, P., Wang, Q., 2011. Retrieval of leaf biochemical parameters using PROSPECT
685 inversion: A new approach for alleviating ill-posed problems. IEEE Trans. Geosci. Remote
686 Sens. 49, 2499–2506. doi:10.1109/TGRS.2011.2109390

687 Lichtenthaler, H.K., Lang, M., Sowinska, M., Heisel, F., Miehé, J.A., 1996. Detection of
688 Vegetation Stress Via a New High Resolution Fluorescence Imaging System. J. Plant
689 Physiol. 148, 599–612. doi:10.1016/S0176-1617(96)80081-2

690 Lu, C., Zhang, J., 2000. Photosynthetic CO2 assimilation, chlorophyl fluorescence and
691 photoinhibition as affected by nitrogen deficiency in maize plants. Plant Sci. 151, 135–143.

692 Mahajan, G.R., Sahoo, R.N., Pandey, R.N., Gupta, V.K., Kumar, D., 2014. Using
693 hyperspectral remote sensing techniques to monitor nitrogen, phosphorus, sulphur and
694 potassium in wheat (Triticum aestivum L.). Precis. Agric. 15, 499–522.
695 doi:10.1007/s11119-014-9348-7

696 Mahajan, G.R., Pandey, R.N., Sahoo, R.N., Gupta, V.K., Datta, S.C., Kumar, D., 2016.
697 Monitoring nitrogen, phosphorus and sulphur in hybrid rice (Oryza sativa L.) using
698 hyperspectral remote sensing. Precis. Agric. 1–26. doi:10.1007/s11119-016-9485-2

699 Meroni, M., Busetto, L., Colombo, R., Guanter, L., Moreno, J., Verhoef, W., 2010.
700 Performance of Spectral Fitting Methods for vegetation fluorescence quantification.
701 Remote Sens. Environ. 114, 363–374. doi:10.1016/j.rse.2009.09.010

702 Moya, I., Camenen, L., Evain, S., Goulas, Y., Cerovic, Z.G., Latouche, G., Flexas, J.,
703 Ounis, A., 2004. A new instrument for passive remote sensing: 1. Measurements of
704 sunlight-induced chlorophyll fluorescence. Remote Sens. Environ. 91, 186–197.
705 doi:10.1016/j.rse.2004.02.012

706 Nobel, P.S., 2009. Photochemistry of Photosynthesis. Physicochem. Environ. Plant Physiol.
707 229–275. doi:10.1016/B978-0-12-374143-1.00005-3

708 Pimstein, A., Karnieli, A., Bansal, S.K., Bonfil, D.J., 2011. Exploring remotely sensed
709 technologies for monitoring wheat potassium and phosphorus using field spectroscopy. F.
710 Crop. Res. 121, 125–135. doi:10.1016/j.fcr.2010.12.001

711 Plascyk, J.A., Gabriel, F.C., 1975. The Fraunhofer line discriminator MKII an airborne
712 instrument for precise and standardized ecological luminescence measurement. IEEE
713 Trans. Instrum. Meas. 24, 306–313. doi:10.1109/TIM.1975.4314448

714 Quemada, M., Gabriel, J.L., Zarco-Tejada, P., 2014. Airborne hyperspectral images and
715 ground-level optical sensors as assessment tools for maize nitrogen fertilization. Remote
716 Sens. 6, 2940–2962. doi:10.3390/rs6042940

717 Ranjan, R., Chopra, U.K., Sahoo, R.N., Singh, A.K., Pradhan, S., 2012. Assessment of
718 plant nitrogen stress in wheat ( Triticum aestivum L.) through hyperspectral indices. Int. J.
719 Remote Sens. 33, 6342–6360. doi:10.1080/01431161.2012.687473

720 Rascher, U., Alonso, L., Burkart, A., Cilia, C., Cogliati, S., Colombo, R., Damm, A.,
721 Drusch, M., Guanter, L., Hanus, J., Hyvärinen, T., Julitta, T., Jussila, J., Kataja, K.,
722 Kokkalis, P., Kraft, S., Kraska, T., Matveeva, M., Moreno, J., Muller, O., Panigada, C.,
723 Pikl, M., Pinto, F., Prey, L., Pude, R., Rossini, M., Schickling, A., Schurr, U.,
724 Schüttemeyer, D., Verrelst, J., Zemek, F., 2015. Sun-induced fluorescence - a new probe of
725 photosynthesis: First maps from the imaging spectrometer HyPlant. Glob. Chang. Biol. 21,
726 4673–4684. doi:10.1111/gcb.13017

727 Ravier, C., Quemada, M., Jeuffroy, M.-H., 2017. Use of a chlorophyll meter to assess
728 nitrogen nutrition index during the growth cycle in winter wheat. F. Crop. Res. 214, 73–82.
729 doi:10.1016/j.fcr.2017.08.023

730 R Core Team. R: A language and environment for statistical computing. R Foundation for
731 Statistical Computing, 2015. Vienna, Austria. http://www.R-project.org/.

732 Rondeaux, G., Steven, M., Baret, F., 1996. Optimization of soil-adjusted vegetation
733 indices. Remote Sens. Environ. 55, 95–107. doi:10.1016/0034-4257(95)00186-7

734 Roujean, J.L., Breon, F.M., 1995. Estimating PAR absorbed by vegetation from
735 bidirectional reflectance measurements. Remote Sens. Environ. 51, 375–384.
736 doi:10.1016/0034-4257(94)00114-3

737 Rouse, J.W., Hass, R.H., Schell, J.A., Deering, D.W., 1973. Monitoring vegetation systems
738 in the great plains with ERTS. Third Earth Resour. Technol. Satell. Symp. 1, 309–317.
739 doi:citeulike-article-id:12009708

740 Sadras, V.O., 2004. Yield and water-use efficiency of water- and nitrogen-stressed wheat
741 crops increase with degree of co-limitation. Eur. J. Agron. 21, 455–464.
742 doi:10.1016/j.eja.2004.07.007

743 Schächtl, J., Huber, G., Maidl, F.-X., Sticksel, E., Schulz, J., Haschberger, P., 2005. Laser-
744 Induced Chlorophyll Fluorescence Measurements for Detecting the Nitrogen Status of
745 Wheat (Triticum aestivum L.) Canopies. Precis. Agric. 6, 143–156. doi:10.1007/s11119-
746 004-1031-y

747 Schlerf, M., Atzberger, C., 2006. Inversion of a forest reflectance model to estimate
748 structural canopy variables from hyperspectral remote sensing data. Remote Sens. Environ.
749 100, 281–294. doi:10.1016/j.rse.2005.10.006

750 Serrano, L., Penuelas, J., Ustin, S.L., 2002. Remote sensing of nitrogen and lignin in
751 Mediterranean vegetation\rfrom AVIRIS data:\rDecomposing biochemical from structural
752 signals. Remote Sens. Environ. 81, 355–364.

753 Smith, G.M., Milton, E.J., 1999. The use of the empirical line method to calibrate remotely
754 sensed data to reflectance. Int. J. Remote Sens. 20, 2653–2662.
755 doi:10.1080/014311699211994

756 Stroppiana, D., Boschetti, M., Brivio, P.A., Bocchi, S., 2009. Plant nitrogen concentration
757 in paddy rice from field canopy hyperspectral radiometry. F. Crop. Res. 111, 119–129.
758 doi:10.1016/j.fcr.2008.11.004

759 Thorp, K.R., Wang, G., West, A.L., Moran, M.S., Bronson, K.F., White, J.W., Mon, J.,
760 2012. Estimating crop biophysical properties from remote sensing data by inverting linked
761 radiative transfer and ecophysiological models. Remote Sens. Environ. 124, 224–233.
762 doi:10.1016/j.rse.2012.05.013

763 Tremblay, N., Wang, Z., Cerovic, Z.G., 2012. Sensing crop nitrogen status with
764 fluorescence indicators. A review. Agron. Sustain. Dev. 32, 451–464. doi:10.1007/s13593-
765 011-0041-1

766 Uddling, J., Gelang-Alfredsson, J., Piikki, K., Pleijel, H., 2007. Evaluating the relationship
767 between leaf chlorophyll concentration and SPAD-502 chlorophyll meter readings.
768 Photosynth. Res. 91, 37–46. doi:10.1007/s11120-006-9077-5

769 Vogelmann, J.E., Rock, B.N., Moss, D.M., 1993. Red edge spectral measurements from
770 sugar maple leaves. Int. J. Remote Sens. 14, 1563–1575. doi:10.1080/01431169308953986

771

772 Walker, A.P., Beckerman, A.P., Gu, L., Kattge, J., Cernusak, L.A., Domingues, T.F.,
773 Scales, J.C., Wohlfahrt, G., Wullschleger, S.D., Woodward, F.I., 2014. The relationship of

774 leaf photosynthetic traits - Vcmax and Jmax - to leaf nitrogen, leaf phosphorus, and specific
775 leaf area: A meta-analysis and modeling study. Ecol. Evol. 4, 3218–3235.
776 doi:10.1002/ece3.1173

777 Wang, W., Yao, X., Yao, X., Tian, Y., Liu, X., Ni, J., Cao, W., Zhu, Y., 2012. Estimating
778 leaf nitrogen concentration with three-band vegetation indices in rice and wheat. F. Crop.
779 Res. 129, 90–98. doi:10.1016/j.fcr.2012.01.014

780 Wang, Y., Li, X., Nashed, Z., Zhao, F., Yang, H., Guan, Y., Zhang, H., 2007. Regularized
781 kernel-based BRDF model inversion method for ill-posed land surface parameter retrieval.
782 Remote Sens. Environ. 111, 36–50. doi:10.1016/j.rse.2007.03.007

783 Wang, Z., Skidmore, A.K., Darvishzadeh, R., Heiden, U., Heurich, M., Wang, T., 2015.
784 Leaf Nitrogen Content Indirectly Estimated by Leaf Traits Derived from the PROSPECT
785 Model. IEEE J. Sel. Top. Appl. Earth Obs. Remote Sens. 8, 3172–3182.
786 doi:10.1109/JSTARS.2015.2422734

787 Weis, E., Berry, J.A., 1987. Quantum efficiency of Photosystem II in relation to "energy"-
788 dependent quenching of chlorophyll fluorescence. BBA - Bioenerg. 894, 198–208.
789 doi:10.1016/0005-2728(87)90190-3

790 Yang, X., Tang, J., Mustard, J.F., Lee, J., Rossini, M., Rascher, U., Alonso, L., Burkart, A.,
791 Cilia, C., Cogliati, S., Colombo, R., Damm, A., Drusch, M., Guanter, L., Hanus, J.,
792 Hyvärinen, T., Julitta, T., Jussila, J., Kataja, K., Kokkalis, P., Kraft, S., Kraska, T.,
793 Matveeva, M., Moreno, J., Muller, O., Panigada, C., Pikl, M., Pinto, F., Prey, L., Pude, R.,
794 Rossini, M., Schickling, A., Schurr, U., Schüttemeyer, D., Verrelst, J., Zemek, F., Houborg,
795 R., Cescatti, A., Migliavacca, M., Kustas, W.P., Genty, B., Briantais, J.M., Baker, N.R.,

796 2015. Satellite retrievals of leaf chlorophyll and photosynthetic capacity for improved
797 modeling of GPP. Agric. For. Meteorol. 990, 10–23. doi:10.1111/gcb.13017

798 Yebra, M., Chuvieco, E., 2009. Linking ecological information and radiative transfer
799 models to estimate fuel moisture content in the Mediterranean region of Spain: Solving the
800 ill-posed inverse problem. Remote Sens. Environ. 113, 2403–2411.
801 doi:10.1016/j.rse.2009.07.001

802 Zarco-Tejada, P.J., Berjón, A., López-Lozano, R., Miller, J.R., Martín, P., Cachorro, V.,
803 González, M.R., De Frutos, A., 2005. Assessing vineyard condition with hyperspectral
804 indices: Leaf and canopy reflectance simulation in a row-structured discontinuous canopy.
805 Remote Sens. Environ. 99, 271–287. doi:10.1016/j.rse.2005.09.002

806 Zarco-Tejada, P.J., Berjon, A., Miller, J.R., 2004. Stress Detection in Crops with
807 Hyperspectral Remote Sensing and Physical Simulation Models. Airborne Imaging
808 Spectrosc. Work. 1–5.

809 Zarco-Tejada, P.J., Catalina, A., González, M.R., Martín, P., 2013. Relationships between
810 net photosynthesis and steady-state chlorophyll fluorescence retrieved from airborne
811 hyperspectral imagery. Remote Sens. Environ. 136, 247–258.
812 doi:10.1016/j.rse.2013.05.011

813 Zarco-Tejada, P.J., González-Dugo, V., Berni, J.A.J., 2012. Fluorescence, temperature and
814 narrow-band indices acquired from a UAV platform for water stress detection using a
815 micro-hyperspectral imager and a thermal camera. Remote Sens. Environ. 117, 322–337.
816 doi:10.1016/j.rse.2011.10.007

817 Zarco-Tejada, P.J., González-Dugo, M. V., Fereres, E., 2016. Seasonal stability of
818 chlorophyll fluorescence quantified from airborne hyperspectral imagery as an indicator of
819 net photosynthesis in the context of precision agriculture. Remote Sens. Environ. 179, 89–
820 103. doi:10.1016/j.rse.2016.03.024

821 Zarco-Tejada, P.J., Miller, J.R., Noland, T.L., Mohammed, G.H., Sampson, P.H., 2001.
822 Scaling-up and model inversion methods with narrowband optical indices for chlorophyll
823 content estimation in closed forest canopies with hyperspectral data. IEEE Trans. Geosci.
824 Remote Sens. 39, 1491–1507. doi:10.1109/36.934080.